國 立 交 通 大 學

顯示科技研究所

碩士論文

非晶與微晶矽鍺合金作為薄膜太陽能電池吸收層之特性分析與最佳化

Characterization and Optimization of Amorphous and Microcrystalline Silicon-Germanium Alloys as Absorber Layers for Thin-Film Solar Cell Applications

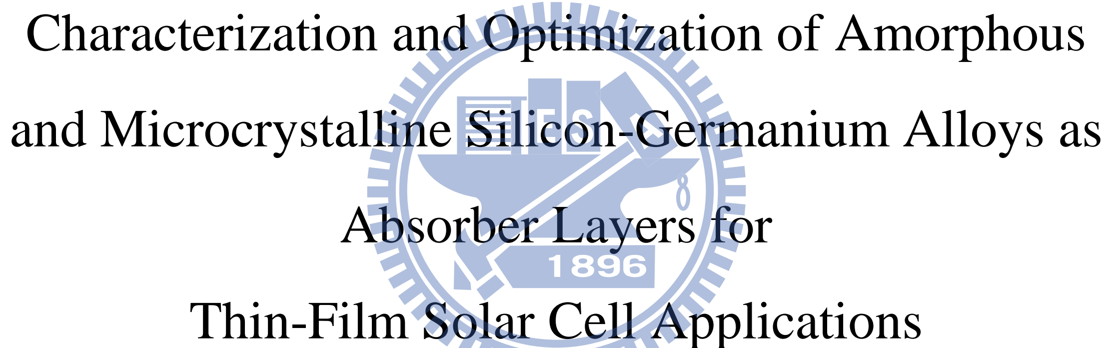

研究生：許宏榮 Hung-Jung Hsu

指導教授：蔡娟娟 教授 Prof. C.C. Tsai

中華民國九十九年八月

非晶與微晶矽鍺合金作為薄膜太陽能電池吸收層

之特性分析與最佳化

Characterization and Optimization of Amorphous and Microcrystalline Silicon-Germanium Alloys as Absorber Layers for Thin-Film Solar Cell Applications

研究生：許宏榮 Student：Hung-Jung Hsu

指導教授：蔡娟娟 教授 Advisor：Prof. C.C. Tsai

國 立 交 通 大 學

顯示科技研究所

碩士論文

A Thesis

Submitted to Display Institute

College of Electrical Engineering and Computer Science

National Chiao Tung University

In partial Fulfillment of the Requirements

For the Degree of Master

In Display Institute

July 2010

Hsinchu, Taiwan, Republic of China

中華民國九十九年八月

非晶與微晶矽合金作為薄膜太陽能電池吸收層之

特性分析與最佳化

研究生：許宏榮　　　　　　　　　　　　**指導教授：蔡娟娟 教授**

國立交通大學顯示科技研究所

中文摘要

在本研究中，藉著改變氫流率、電漿功率以及製程氣體來研究非晶矽鍺與微晶矽鍺之薄膜特性以及非晶矽鍺單接面太陽電池之轉換效率。製程氣體我們使用矽甲烷(SiH_4)、鍺甲烷(GeH_4)以及氫氣，利用射頻電漿輔助化學氣相沉積系統(PECVD)來沉積非晶矽鍺薄膜。由本篇實驗發現通入適當氫氣可提升光電導，而鍺原子濃度亦影響光學能隙以及電性。電漿功率除了會影響薄膜沉積速率外同時亦可提升電性。在元件的表現上可分為以下幾個部分：非晶矽鍺吸收層的厚度大約在 150 nm 至 300 nm 之間為佳，過厚或過薄都會對效率有不良影響；較高的沉積功率增強了對表面的離子轟擊效應因此讓元件填充因子下降；在 p/i 與 i/n 介面間加入一緩衝層可有效阻擋磷原子擴散至吸收層，使得界面品質改善；最後，當我們將吸收層中的鍺含量做漸變的變化，元件有較大的開路電壓且效率可達 8.5 %。

在微晶矽鍺合金方面，當我們逐漸提升沉積時的放電功率可發現一個由非晶矽鍺合金轉變到微晶矽鍺合金的區域，且越接近此轉變的區間，膜中的結晶範圍越大。調整氫氣稀釋比例也可改變膜中的結晶率，但由光暗電導可發現此時的膜大多為高度結晶。改變膜中的鍺含量會大幅影響微晶矽鍺薄膜的特性，氣態的鍺濃度大約在 9 % 至 16 % 為最佳的區間，光暗電導的差距約為一至兩個數量級。

Characterization and Optimization of Amorphous and Microcrystalline Silicon-Germanium Alloys as Absorber Layers for Thin-Film Solar Cell Applications

Master Student: Hung-Jung Hsu **Advisor: Dr. Chuang-Chuang Tsai**

Display Institute

National Chiao Tung University

Abstract

In this study, the effects of systematic variation in hydrogen dilution, RF power, gas phase ratio of germane (R_{GeH4}) on the hydrogenated amorphous silicon germanium (a-SiGe:H) and hydrogenated microcrystalline silicon germanium (μc-SiGe:H) alloys properties and a-SiGe:H single junction solar cell performance have been studied. The a-SiGe:H and μc-SiGe:H films were deposited from the mixture of SiH_4, GeH_4 , and H_2 dilution by the plasma enhanced chemical vapor deposition (PECVD) system at 27.12 MHz. It has been found that hydrogen dilution plays an important role in the properties of films. Adequate hydrogen dilution ratio can improve the photo photosensitivity, but both higher and lower hydrogen dilution ratio deteriorates the film properties. Power density influences on the deposition rate and electronic properties. Photo conductivity is higher for films deposited at higher power density for all hydrogen dilution ratios. Dark conductivity is almost the same for films deposited at two different power densities for all hydrogen dilution ratios. The device performance is better for the cell deposited at 20 W then 30 W, which means that ion bombardment plays a more important role than i-layer film quality.

Acknowledgements

回顧這兩年來的點點滴滴，這篇論文能夠順利完成，的確要感謝許許多多的人，有了你們的幫助，我才能在研究的路上稍有斬獲。

首先我要感謝的是 蔡娟娟教授，感謝老師帶我進入太陽能的研究領域，並在研究的路上給予我許多幫助 ，尤其是當我在面臨抉擇時，老師不吝給我指引，讓我思考得更周全能夠穩健的踏出下一步，非常感謝您!

其次我要感謝國錫學長，感謝學長在我的研究領域給予我非常多的指導與幫助，從您身上我學到了不只是專業的知識，更多的是您讓我看到了一位專注在研究與開發的工作者應有的典範，我會盡量以您為目標並繼續前進！

再來我要感謝建敏學長，在我碩一的時候您總是替我規畫好大大小小的事，並且很願意撥空教我做實驗的方式甚至是和我溝通很多觀念，讓我能夠順著您的腳步，慢慢的將自己轉換到一位研究生的角色，真的很感謝您，謝謝!

我要特別感謝振航學長，感謝您在管理實驗室上付出了相當多的努力，並謝謝您總是給予我很多在研究上的幫助，每次跟您討論完都有一種踏實且安心的感覺，尤其在論文修改方面也提供我很多寶貴的意見，希望接下來能在你身上學到更多的東西!

接著我要感謝鵬鵬、柏翔、建亞等三位好朋友，感謝你們一直很照顧我，一起做實驗量測討論報告改進打球唱歌的日子真是令人懷念，我覺得你們真是優秀的一群，相信你們不管到哪裡都會表現得很出色的，希望我們能一直保持聯絡!

感謝辛瑋學長時常提點我許多做人的道理，您成熟、不屈不撓又穩重是我要學習的目標，和您打球很開心；感謝彥棠學長在研究上給予我的幫助，總是讓我能夠多思考一個問題不同的面向；感謝碩一的各位，智凱、怡萍及奕文，感謝你

們時常主動的幫我們準備實驗的材料，讓我們能專心在研究上，並且讓實驗室氣氛更溫馨和諧；感謝世益、伍佰、琇文、明哲提供了我在實驗上的幫助，也讓實驗室一直存在歡笑；感謝威豪、達欣、芳弘三位學長為實驗室打下良好的基礎，並且教導我實驗的技巧，讓我能夠很快的熟悉各種機台的操作，有你們在的實驗室總是充滿歡笑聲；感謝慶能、煥之、淑玲、鈞銘等學長姐在實驗上給予的協助，希望有機會能再跟你們打個球敘敘舊；感謝奇美能源的前輩們，讓我學到很多開發元件的邏輯跟技巧，特別感謝育華在實驗及規劃方面給我的協助，讓我學到很多；感謝田仲豪老師在光學理論上給我的指引；感謝林怡欣老師精彩的講課讓我有幸能學會一些有關光學理論的概念，並且感謝您在我面臨抉擇的時候不吝給予我建議，非常感謝您!

感謝口試委員張正陽教授、陳方中教授、冉曉雯教授在百忙之中撥冗前來參與口試並提供許多寶貴意見使論文能夠更臻於完善。

此外我還要感謝奈米中心的何惟梅小姐、林聖欽先生、黃國華先生，優貝克的陳江耀以及張智皓先生，謝謝你們在實驗上給予我各種幫忙。也感謝光電所的助理張欣恆小姐、古明嫣小姐、張雅惠小姐以及童雅玲小姐在行政業務上幫了我許多忙。

我要感謝一直以來陪伴在我身邊的宜蓉，妳是最了解我的人，當我疲累時總是支持著我的內心，還要時常包容我的孩子氣，很多事情多虧了妳才讓我做出正確的選擇，感謝妳陪我完成了各種大大小小的事，我會變得更成熟的，謝謝妳!

最後，我要感謝我的父母親 許家豪先生、黃鈺雯女士，感謝您們一直以來都尊重我的想法，傾聽我所遇到的困難並且給我很多的關懷，讓我能順利完成碩士學業，希望我能夠早日成為一個獨當一面的人，謝謝你們！

List of Tables

Table 3.1 Vibration frequencies of SiHx(x=1~3) in a-Si:H [33] 20

Table 4.1 Illuminated J-V parameters of a-$Si_{1-x}Ge_x$:H single junction solar cells with different combination of back contact material. 41

List of Figures

Fig 1.1 The change in the global energy composition until 2050/2100 1

Fig 1.2 The progress of the best research-cell conversion efficiencies.........2

Fig 1.3 Absorption coefficient, α, versus Photon energy for a-Si:H, μc-Si:H and c-Si..5

Fig 1.4 Schematic diagram of a single junction a-Si:H p-i-n solar cell structure...6

Fig 2.1 Band diagram and sketch of (a)a p-n and (b)a p-i-n cells[4] 10

Fig 2.2 The atomic structure of (a) crystalline silicon (b) hydrogenated amorphous silicon and (c) hydrogenated amorphous silicon germanium alloy...11

Fig 2.3 Schematic representation of the rf PECVD system. 13

Fig 3.1 Photo energy (ħω) as function of the αħω and the tauc band gap 17

Fig 3.2 Micro-Raman spectrometer composed of an He-Ne laser source, a microscope, a notch filter, a grating and a CCD camera [26]........18

Fig 3.3 Raman spectrum of a μc-Si:H sample...19

Fig 3.4 Schematics of the conductivity measurement.................................21

Fig 3.5 Schematic of air mass 22

Fig 4.1 (a) The deposition rate (b) The bonding intensity ratio, as a function of R_{H2} for three different R_{GeH4} at 8.3, 11.1, 16.7% 26

Fig 4.2 Fourier transform infrared spectra of a-$Si_{1-x}Ge_x$:H alloys with

different R_{H2} = 0-3 at R_{GeH4} = 8.3% 27

Fig 4.3 The dependence of photoconductivity and dark conductivity of a-$Si_{1-x}Ge_x$:H alloys on R_H at various X_g 28

Fig 4.4 Dependence of the photo-to-dark conductivity ratio with hydrogen dilution ratio. 28

Fig 4.5 The dependence of optical band gap of a-$Si_{1-x}Ge_x$:H alloys on R_{H2} at various R_{GeH4} 29

Fig 4.6 (a) Enhancement factor and (b) Ge content in a-$Si_{1-x}Ge_x$:H alloys as a function of R_H for three various X_g at 8.3, 11.1, 16.7% 30

Fig 4.7 Hydrogen content as a function of hydrogen dilutiob ratio at different three germane concentrations. 31

Fig 4.8 Dependence of the photo-conductivity (σ_{ph}) and dark-conductivity (σ_d) with hydrogen dilution ratio 32

Fig 4.9 Illuminated J-V characteristics of 216-nm-thick a-$Si_{1-x}Ge_x$:H single junction solar cells prepared with one or two buffer layer. 34

Fig 4.10 QE spectra of a 216-nm-thick a-$Si_{1-x}Ge_x$:H single junction solar cell under zero bias and -0.5 V bias. 35

Fig 4.11 Illuminated J-V characteristics of a-$Si_{1-x}Ge_x$:H single junction solar cells with i layer prepared with 20 W and 30 W. 36

Fig 4.12 Illuminated J-V characteristics of a-$Si_{1-x}Ge_x$:H single junction solar cells with different i layer thickness (180 nm and 226 nm). 38

Fig 4.13 Illuminated J-V characteristics of a-$Si_{1-x}Ge_x$:H single junction solar cells prepared with different i layer thickness 39

Fig 4.14 Dependence of V_{OC}, J_{SC}, FF and Efficiency of a-$Si_{1-x}Ge_x$:H single junction solar cells on i layer thickness. 40

Fig 4.15 **Illuminated J-V characteristics of 216-nm-thick a-$Si_{1-x}Ge_x$:H single junction solar cells with different combination of back contact material.** 41

Fig 4.16 **Illuminated J-V characteristics of 216-nm-thick a-$Si_{1-x}Ge_x$:H single junction solar cells post-annealed at various temperature (T_S= 145 ^{O}C, 150 ^{O}C, 155 ^{O}C, 160 ^{O}C).** 43

Fig 4.17 **Dependence of V_{OC}, J_{SC}, FF and Efficiency of a 216-nm-thick a-$Si_{1-x}Ge_x$:H single junction solar cell on post-annealing temperature.** 43

Fig 4.18 **Illuminated J-V characteristics of a-$Si_{1-x}Ge_x$:H single junction solar cells prepared with constant and graded GeH_4 concentration.** 45

Fig 4.19 **Illuminated J-V characteristics of a-$Si_{1-x}Ge_x$:H single junction solar cells prepared with constant and different graded GeH_4 concentrations.** 46

Fig 4.20 **Raman scattering spectra for μc-$Si_{1-x}Ge_x$ films deposited on bare glass at fixed germane concentration (R_{GeH4}) with various power ranging from 100 W to 600 W.** 48

Fig 4.21 **Dark conductivities (solid symbols) and photo conductivities (open symbols) as a function of discharge power.**....49

Fig 4.22 **XRD spectra of μc-$Si_{1-x}Ge_x$ films deposited on bare glass at fixed germane concentration (R_{GeH4}) with various power ranging from 100 W to 600 W.**....50

Fig 4.23 **Raman scattering spectra of μc-$Si_{1-x}Ge_x$ films deposited on bare glass at different hydrogen dilution ratio (R_{H2}) ranging from 95.3**

1896

% to 98.9 %. The other deposition parameters were kept unchanged.......51

Fig 4.24 Dark conductivities (solid symbols) and photo conductivities (open symbols) as a function of hydrogen dilution ratio (R_{H2}).......52

Fig 4.25 Raman scattering spectra of μc-$Si_{1-x}Ge_x$ films deposited on bare glass at different germane concentrations (R_{GeH4}) ranging from 9.1 % to 33.3 %. The μc-Si:H film is also shown for comparison. 53

Fig 4.26 Dark conductivities (solid symbols) and photo conductivities (open symbols) as a function of germane concentration (R_{GeH4}).......54

Fig 4.27 Raman scattering spectra of μc-$Si_{1-x}Ge_x$ films deposited on bare glass at different germane concentrations (R_{GeH4}) ranging from 3.8 % to 16.7%. 55

Fig 4.28 Dark-conductivities (solid symbols) and photo-conductivities (open symbols) as a function of germane concentration (R_{GeH4}).......56

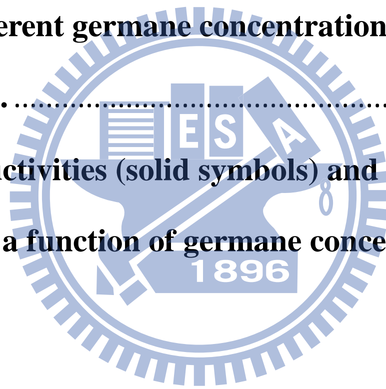

Contents

中文摘要 .... **I**

Abstract .... **II**

Acknowledgements .... **III**

List of Tables .... **V**

List of Figures .... **VI**

Chapter 1 Introduction **1**

1.1 Global Warming and Energy Resource Problem 1

1.2 Introduction to Photovoltaic (PV) Technology 2

1.2.1 Current Development of PV Technology 2

1.2.2 Thin Film Solar Cell Technology 3

1.2.3 Si Thin-Film Solar Cell 5

1.3 Motivation 7

Chapter 2 Literature Review **8**

2.1 Introduction 8

2.2 P-i-n Structure of Silicon Based Solar Cell 9

2.3 Hydrogenated Amorphous Silicon 10

2.3.1 Material Properties 10

2.3.2 Stabler-Wronski Effect 12

2.3.3 Hydrogenated Amorphous Silicon-Germanium Alloys 12

2.4 Radio-Frequency Plasma-Enhanced Chemical Vapor Deposition 13

2.5 Hydrogenated Microcrystalline Silicon 15

ES A 1896

2.5.1 Material Properties 15

2.5.2 Hydrogenated Microcrystalline Silicon-Germanium Alloys 16

Chapter 3 Experimental Details 17

3.1 Material Characterization... 17

3.1.1 Reflection-Transmission Spectroscopy.. 17

3.1.2 Raman Spectroscopy... 17

3.1.3 Fourier Transform Infrared Spectroscopy (FTIR) 19

3.1.4 X-Ray Diffraction (XRD) 20

3.1.5 I-V Measurement 20

3.2 Solar Cell Characterization 21

3.2.1 AM 1.5 Light Source 21

3.2.2 Current-Voltage Characteristics 23

3.2.3 Quantum Efficiency 24

Chapter 4 Results and Discussions 25

4.1 Deposition and Characterization of a-SiGe Thin-Films 25

4.1.1 The Effect of Hydrogen Dilution on Deposition Rate and Film Quality 25

4.1.2 The Effect of Hydrogen Dilution on Conductivity Properties 27

4.1.3 The Effect of Hydrogen Dilution on Optical Bandgap and Ge Atom Concentration 29

4.1.4 The Effect of RF Power on Film Quality.................................... 31

4.2 a-SiGe:H Single Junction Solar Cell Optimization 32

4.2.1 Effect of Buffer Layer on Cell performance 32

4.2.2 RF Power Effect on cell performance.. 35

4.2.3 Thickness Variation for p+/b/i/b/n+ Structure 36

4.2.4 Layer Thickness Variation with Elevated Ge Incorporation........38

4.2.5 Back Contact Comparison 40

4.2.6 Anneal Temperature Optimization..42

4.2.7 Bandgap Engineering...44

4.2.8 n-layer Thickness Variation 46

4.3 Deposition of μc-SiGe:H Thin-Film and Performance of Solar Cells.....47

4.3.1 Effect of RF Power on Film Quality..47

4.3.2 Effect of Hydrogen Dilution on Conductivity 50

4.3.3 Effect of GeH_4 Concentration on Conductivity..........................52

Chapter 5 Conclusions...57

Chapter 6 Future Works...59

Chapter 7 References 61

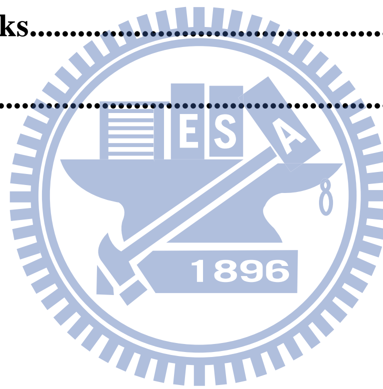

Chapter 1 Introduction

1.1 Global Warming and Energy Resource Problem

The global warming has already caused many worldwide disasters including floods, droughts, and the related problems like contagions and famine. Based on many research groups' investigations, such as Intergovernmental Panel on Climate Change (IPCC), there is an apparent relationship between the carbon dioxide concentration and global temperature. The biggest source of carbon dioxide is the utilization of fossil fuel, especially in the energy field. Thus, in order to lower the damage to our environment, developing clean and renewable energy is one effective approach. Among various energy sources, photovoltaic (solar power) has the advantages of pollution-free during use and the lasting energy input from the sun, making photovoltaic one of the most

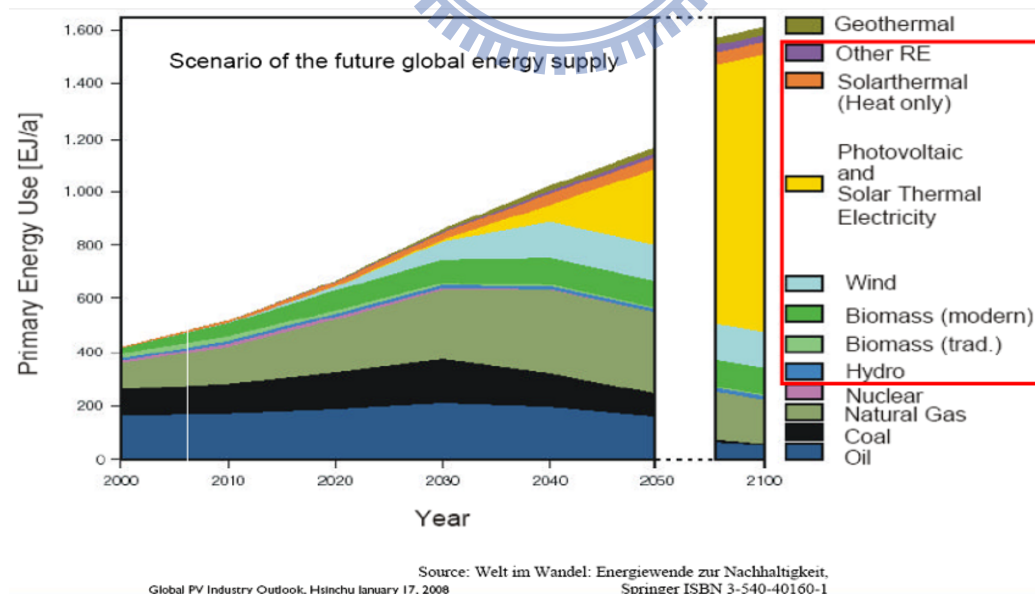

Fig 1.1 The change in the global energy composition until 2050/2100

promising clean energy method. As shown in **Fig 1.1**, based on the prediction of

German Advisory Council on Global Change (WBGU), solar power will be one of the highest-growing and the dominant energy resource in the future 100 years.

1.2 Introduction to Photovoltaic (PV) Technology

1.2.1 Current Development of PV Technology

There are three generations of solar cells. The first generation is silicon (Si) wafer-based solar cell, which is with higher conversion efficiency but higher costs. The second generation is thin film solar cell, which is with lower costs as well as lower conversion efficiency. The third generation is solar cell with new materials such as organic solar cell or dye-sensitized solar cell, which are still during the laboratory stage.

As shown in **Fig 1.2**, the historical efficiency record released by Nation Renewable Energy Laboratory (NREL) shows that the efficiency of the research-cell is still being improved in various kinds of solar cell. Generally speaking, the higher conversion efficiency often accompanied with higher cost or complicated

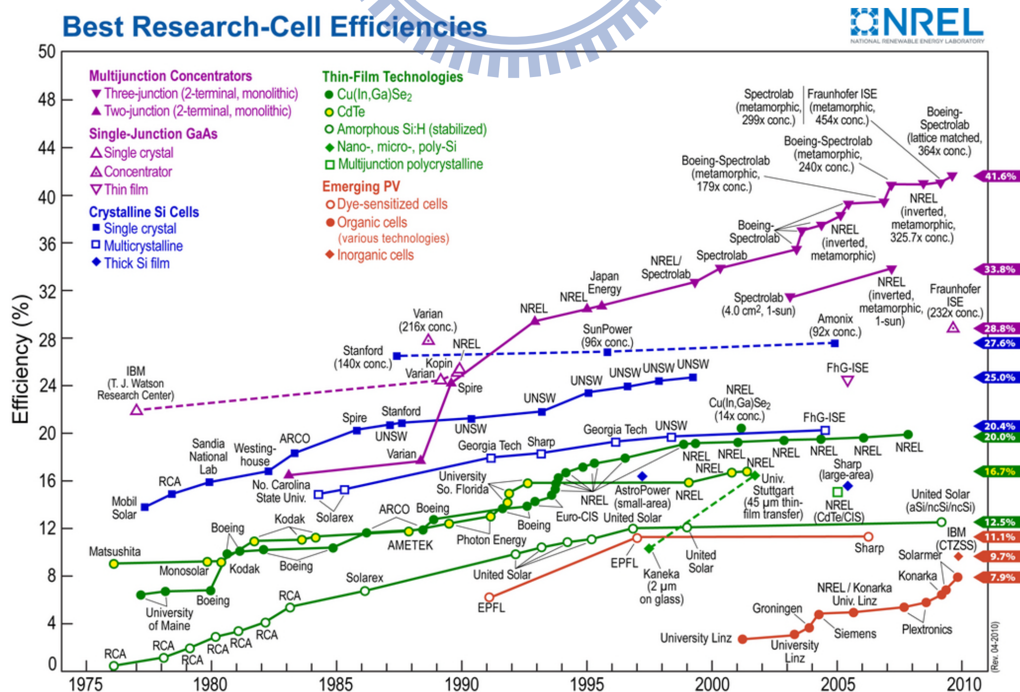

Fig 1.2 The progress of the best research-cell conversion efficiencies

fabrication process. The goal of grid-parity can only be achieved when the cost per watt is low enough compared to current fossil fuel.

Among various kinds of solar cell technologies, the most common solar cell is a crystalline silicon (c-Si) p-n junction. The Si atoms in this type are periodically arranged. High efficiency c-Si solar cell needs high quality and purity wafer, making the cost become higher. Also, the optical absorption coefficient of c-Si solar cell is low since Si is indirect band-gap material, which means the thickness should be thick enough to absorb photons. Once the price of c-Si rises, this high material consumption must increase the total cost of solar cell fabrication.

Compared to c-Si solar cell, thin-film solar cell technology is currently developed to reduce the amount of light absorbing material. Also, it is carried out at lower temperature, making it possible to deposit on cheaper or flexible substrates such as glass or plastic substrate. In addition to low cost and flexibility, thin film solar cell technology has advantages including lighter weight and ease of integration compared to wafer silicon. Due the above benefits, thin-film solar cell is a promising category of solar cells in the energy field.

1.2.2 Thin Film Solar Cell Technology

There are several categories in thin film solar cell technology including Si thin film, cadmium telluride (CdTe), copper indium selenide/ copper indium gallium selenide (CIS/CIGS), and Organic/polymer solar cell. The following are some introduction and characteristics about these thin film solar cells:

CdTe solar cells: With an optimal band-gap of 1.44 eV, CdTe is an efficient light-absorbing material for thin film cells. The cell thickness of nearly one micron is

enough to absorb photons, therefore, the material costs is significantly reduced. Efficiencies close to 10% have been achieved in commercial modules by Solar Cells Inc. However, the toxicity of CdTe-based solar cell on health and the environment is still a concern.

CIS/CIGS solar cells: These semiconductors are attractive materials due to their high optical absorption coefficient and versatile optical and electrical characteristics so that they can be manipulated to fit the needs for device. The best efficiency of CIGS solar cell has achieved 19.9% in 2008 [1]. By using optical concentrator or multi-junction tandem solar cell, higher efficiencies (>30%) can be obtained. But the manufacturing costs of CIGS solar cells are high when compared to amorphous silicon (a-Si) solar cells.

Organic/polymer solar cell: These devices don't rely on built-in electric field like inorganic solar cells. The active layer consists of two materials, one acts as an electron donor and the other as an acceptor. The efficiencies of organic/polymer solar cell has quickly improved in recent years and the best one is 6.77% [2]. But the stability and excitation diffusion length should be enhanced in the future.

Si thin film solar cells: Si is the top two abundant element in earth's crust (only less than oxygen), and it makes up 25.7% of the crust by mass. That is the reason why Si-based solar cells are the most well-studied alternative energy method. Meanwhile, thin-film silicon solar cells such as hydrogenated amorphous silicon (a-Si:H) can be scaled to large area and deposited on various kind of substrates so that it is a promising material in the energy field. Furthermore, the multi-junction technology

based on the concept of spectrum splitting can also be applied to combine a-Si:H with hydrogenated microcrystalline silicon (μc-Si:H) solar cells to enhance absorption. Triple stack a-Si:H/μc-Si:H/μc-Si:H achieved module efficiency of up to 12% with much less photo-degradation [3]. Our group also focuses on this Si thin film solar cells.

1.2.3 Si Thin-Film Solar Cell

Si thin-film solar cells consists of a-Si based solar cells including amorphous silicon germanium (a-SiGe) and μc-Si based solar cells including microcrystalline silicon germanium (μc-SiGe). Compared to c-Si solar cell, the light absorption coefficient of thin film Si materials is much higher, as shown in **Fig 1.3**. Thus, the thickness (~1μm) and Si material consumption can be effectively reduced, which can reduce the fabrication cost of solar cells.

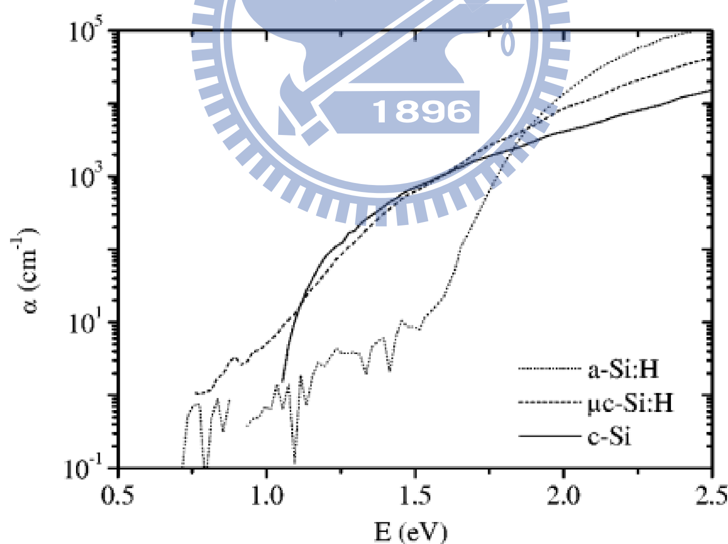

Fig 1.3 Absorption coefficient, α, versus Photon energy for a-Si:H, μc-Si:H and c-Si

Silicon based thin-film solar cells can be fabricated in two configurations: p-i-n or n-i-p. We focus on p-i-n structure in this thesis, as shown in **Fig 1.4**. In this configuration, light enters from the p-layer side. The internal electric field is built up by

the Fermi level difference between p- and n-layer. When light incidence, electron-hole pairs are created in the intrinsic microcrystalline silicon layer (i-layer), which is the "photon absorption" process. Then, "charge separation" happens because of the internal electric field. During the transportation process, "charge recombination" occurs due to defects in the films. Finally, those charges transported longer enough will be collected by the electrodes. "Absorption, transportation, and collection" are the working mechanism for solar cell to convert light to electricity.

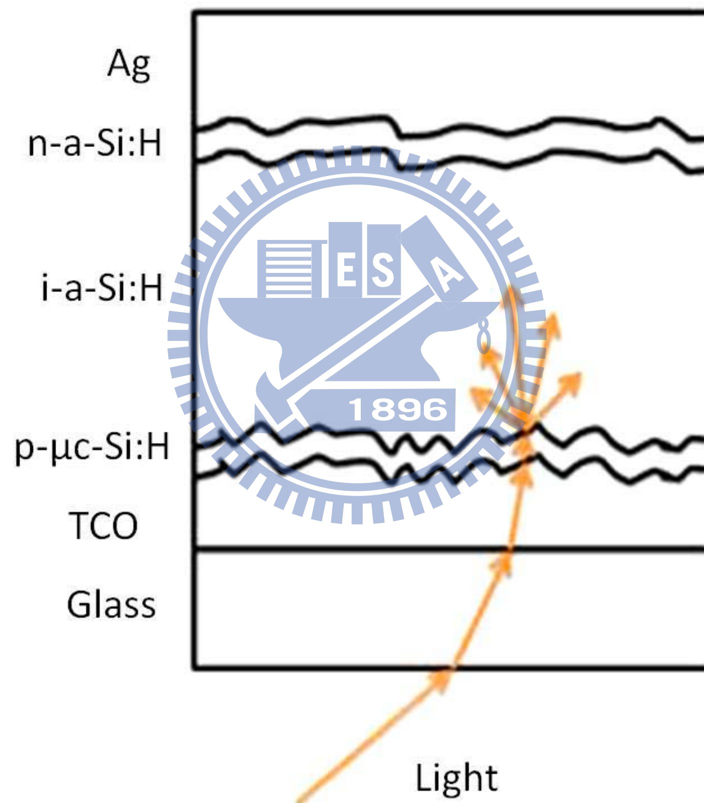

Fig 1.4 Schematic diagram of a single junction a-Si:H p-i-n solar cell structure.

There are several advantages of choosing a-Si:H based material as an absorber materials. First, due to the direct band-gap property, a-Si:H solar cell has higher optical absorption coefficient in visible spectrum. Also, the manufacturing method of a-Si:H is

mature and the cost is low. Besides, thin-films can be deposited on glass, metal or plastic substrates, which extends the application field of thin-film solar cells. But the serious light degradation is the main problem that should be improved.

The structure of μc-Si:H is between a-Si and c-Si, there are some crystalline parts incorporate into amorphous network. Because of such structure, μc-Si:H also possesses the advantages of a-Si:H such as high optical absorption coefficient and low cost. Furthermore, because the presence of crystalline phase, the light degradation of μc-Si:H is much less than that of a-Si:H.

The combination of a-Si:H and μc-Si:H tandem solar cell is a fascinating structure, because the absorption range are wide to cover most visible light spectrum. For a-Si:H, the absorption peak is toward short wavelength; for μc-Si:H, the absorption peak is toward long wavelength. Thus, combination of these two type solar cells could achieve a substantial increase of conversion efficiency due to broader light spectrum absorption.

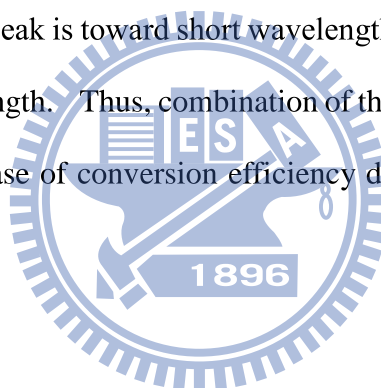

1.3 Motivation

In order to enhance the conversion efficiency as well as to upgrade the performance per cost of silicon solar cell, this series of experiments investigates the characteristics of thin film material. We attempt to understand which material properties could improve the conversion efficiency and endeavor to manipulate these material properties by controlling appropriate process parameters. Consequently, a series of experiment on silicon thin film solar cell have been done in this thesis.

Chapter 2 Literature Review

2.1 Introduction

In 1905, the photoelectric effect was explained by Elbert Einstein. The explanation relies on ideas from quantum theory. Light is made up of a pack of photons, the photon energy depends only on the frequency (or wavelength) of light. When the wavelength of light is smaller than a threshold value (usually blue or ultraviolet light) then radiating at the surface of a metal, the electrons will absorb enough energy to escape completely. The escaping electrons are called photoelectrons. Because the work function of a metal is as high as 3 to 5 eV, so the maximum conversion efficiency of bounded electrons to photoelectrons is lower than 1%. This phenomenon is called as photoelectric effect and cannot be explained by wave theory, that is, the escape capability of bounded electrons depends on the energy of light, not on the intensity of light.

Generally speaking, the energy of photons in visible spectrum is sufficient to excite electrons to higher energy levels where they are easier to move, but the excited electrons will quickly relax back to their ground states. In photovoltaic devices, there is a built-in electric field which can separate photo-generated carriers away and extract them to external circuit. The extra energy of excited electrons generates a potential difference which drives these electrons to external load and does electrical works. This phenomenon is the photovoltaic effect.

2.2 P-i-n Structure of Silicon Based Solar Cell

There are three major mechanisms responsible for the collection of photo-generated carriers in p-n diode photovoltaic:

1. The drift current of holes and electrons in depletion region.
2. The diffusion current of minority carriers in n-type neutral region
3. The diffusion current of minority carriers in p-type neutral region

In typical mono-crystalline and poly-crystalline silicon p-n diode photovoltaic, the contribution of photo-generated carriers in depletion region is trivial due to the width of this region is too thin compared to the diffusion length of minority carriers. The main current of mono-crystalline and poly-crystalline solar cells is the diffusion current in the neutral region. The absorption coefficient of amorphous silicon is about two orders higher than crystalline silicon, the material needed in amorphous silicon thin film solar cells is 1% of crystalline silicon solar cells needed. However, amorphous silicon is a defective material. The diffusion lengths are so short in doped a-Si, the undoped region is needed to extend the thickness which photons can be absorbed effectively. The thin p-layer and n-layer create the built-in field which drives the charges to separate. In the p-i-n structure photo-carriers are collected primarily by drift rather than by diffusion. **Fig 2.1** shows the band diagrams and sketches of p-n and p-i-n structures, respectively.

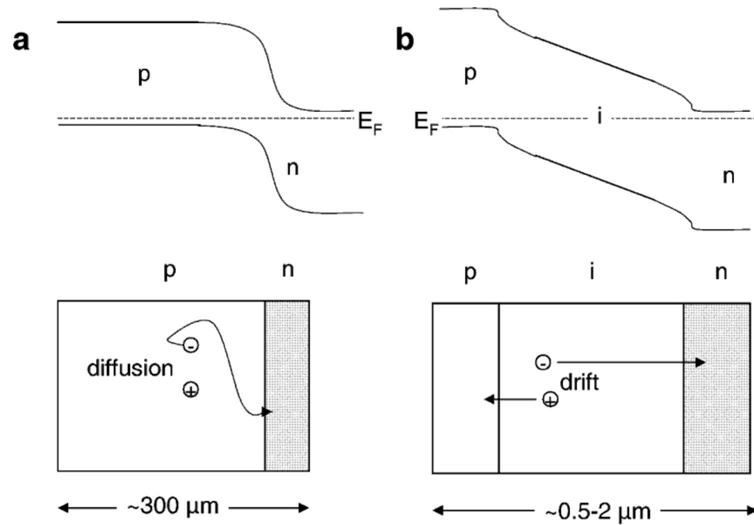

Fig 2.1 Band diagram and sketch of (a)a p-n and (b)a p-i-n cells [4]

2.3 Hydrogenated Amorphous Silicon

The use of amorphous silicon can be retraced to 1965 as films of 'silicon from silane' deposited in a radio frequency glow discharge [5].Ten years later, Walter Spear and Peter LeComber reported that amorphous silicon had semiconducting properties. The conductivity of amorphous silicon can be manipulated by several orders of magnitude by adding some phosphine or diborane into the gas mixture [6]. One year later, Carlson and Wronski announced that they had made the first experimental a-Si:H solar cell at the RCA laboratory in 1976 [7]. The discovery of a-Si:H open a new era to thin film silicon solar cells and related technologies.

2.3.1 Material Properties

Hydrogenated amorphous silicon (a-Si:H) is the non-crystalline allotropic form of silicon. It can be deposited as thin film onto a variety of substrates at low temperatures. Silicon is a four-fold coordinated atom that is normally tetrahedrally bonded to four neighboring silicon atoms. In crystalline silicon this tetrahedral structure is continued

over a large range, forming a well-ordered lattice (crystal), as shown in **Fig 2.2** (a).

In amorphous silicon this long range order is not present and the atoms form a continuous random network. Not all the atoms within amorphous silicon are four-fold coordinated. Due to the disordered nature of the material, some atoms have unpaired electron, which is called dangling bonds. These dangling bonds present as defects or voids in the silicon random network, which cause anomalous electrical behavior.

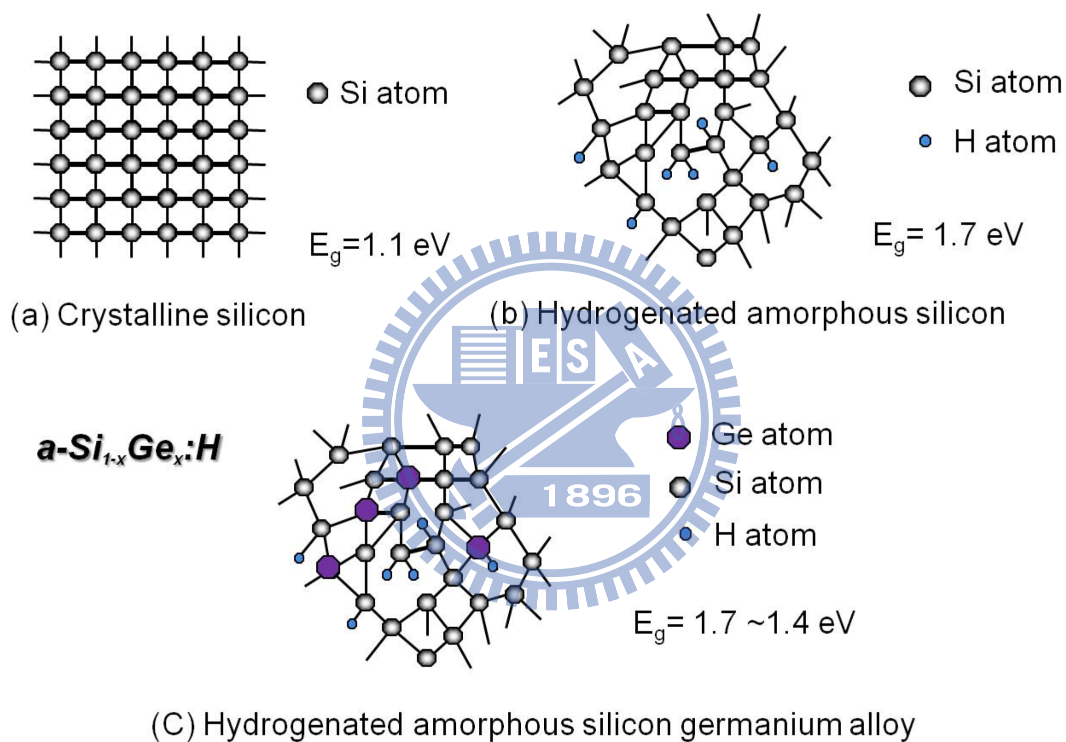

Fig 2.2 The atomic structure of (a) crystalline silicon (b) hydrogenated amorphous silicon and (c) hydrogenated amorphous silicon germanium alloy.

If desired, the material can be passivated by hydrogen which bonds to the dangling bond to reduce the dangling bond density by several orders of magnitude. This phenomenon makes amorphous silicon a useful material that the conductivities can be

manipulated by several orders of magnitude. In general, there exists about 10 at.% hydrogen in hydrogenated amorphous silicon thin film. Hydrogenated amorphous silicon has a sufficiently low amount of defects to be used within devices. However, the hydrogen is unfortunately associated with light-induced degradation of the material, termed the Staebler-Wronski effect.

2.3.2 Stabler-Wronski Effect

Electrical properties of amorphous silicon would be changed under long time light exposure. This phenomenon is well-known as Staebler-Wronski Effect discovered by D. L. Staebler and C. R. Wronski in 1977 [8]. Weak bonds in amorphous silicon like dihydride, trihydride bonds and cluster of Si-H may be broken and result in the formation of dangling bonds by long time illumination of light. When the defect density of dangling bonds increases, the lifetime of photo-generated carriers reduces. Due to the strong recombination loss through the localized states formed by the dangling bonds in amorphous silicon network, the conversion efficiency degraded severely in a-Si:H based solar cells [9-10].

However, an essential feature of light-induced effects on a-Si:H film and solar cell can be reversible by annealing above 150℃. The performance of stabilized a-Si:H solar cells is 70 to 85％ of their initial efficiency depends on the quality of a-Si:H film. This light-induced degradation is the major disadvantage of amorphous silicon as a photovoltaic material.

2.3.3 Hydrogenated Amorphous Silicon-Germanium Alloys

Amorphous silicon alloys are widely used in thin film solar cell technologies, such as a-$Si_{1-x}Ge_x$. Structure of amorphous silicon germanium alloy is shown in figure **Fig**

2.2 (c). Incorporation of germanium adds extra freedom to controlling the properties of the material. Increasing concentration of germanium in the alloy narrows the electric gap between conduction and valence band (called bandgap) and also potentially increases the light absorption coefficient and extends the absorption range of the solar spectrum. However, the electric properties as a semiconductor (mainly electron mobility), are negatively affected by the increasing content of germanium in the alloy, due to the increased disorder in the atomic network.

One advantage is that a-Si and its alloys can be deposited at very low temperatures (~200℃). This allows for deposition not only on glass, but plastic as well, making it a candidate for a roll-to-roll processing technique. Another advantage is that a-Si can be deposited over large areas by PECVD.

2.4 Radio-Frequency Plasma-Enhanced Chemical Vapor Deposition

Plasma-enhanced chemical vapor deposition (PECVD) is a common technique

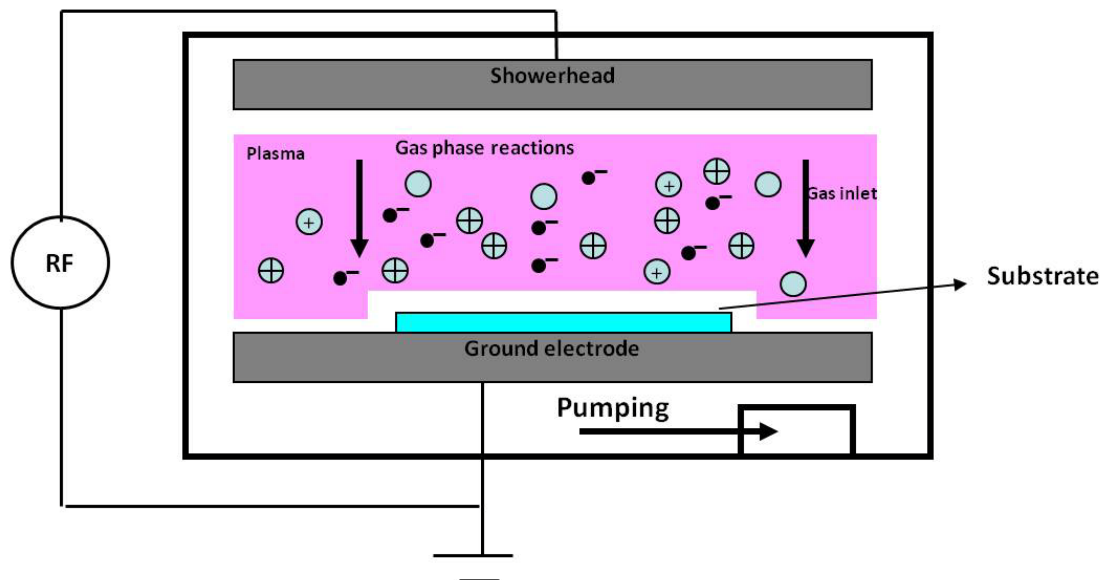

Fig 2.3 Schematic representation of the RF-PECVD system.

used for the manufacturing of most microelectronic devices. The deposition of hydrogenated films at lower temperatures requires a source of energy to dissociate SiH_4 and GeH_4 and this is the role of plasma. This is done by collisions with electrons, which originates as secondary electrons in the plasma to acquire their energy by acceleration in an electric field. The growth of an a-SiGe:H and μc-SiGe:H film is accomplished by attaching reactive particles of dissociated silane and germane molecules, called radicals, to the surface, as sketched in **Fig 2.3**.

Most reactors have been designed in diode configuration in which plasma is confined between two parallel electrodes. Despite being a relatively simple reactor, there are many variables in the deposition process which must be controlled to give good material quality. The gas pressure determines the mean free path for collisions of the gas molecules and influences whether the reactions are at the growing surface or in the gas. The gas flow rate determines the residence time of the gas species in the reactor. The rf power control the rate of dissociation of the gas and therefore also the film growth rate. And the substrate temperature of the substrate controls the chemical reactions on the growing surface.

In the dissociation process, gas molecule will be decomposed into many kinds of neutral radicals or ions. Among these radicals and ions, there are two radicals that possess higher sticking coefficients than other radicals and they would incorporate directly onto the hydrogen terminated surface without finding potential favorable growth site. Therefore, these radicals are usually formed voids in the film resulting in poor film quality. So, the presence of these radicals in the plasma should to be avoided.

2.5 Hydrogenated Microcrystalline Silicon

2.5.1 Material Properties

The definition of hydrogenated microcrystalline silicon (μc-Si:H), based on the study done by Schropp [11], is a two-phase material including amorphous part and crystalline part with crystal sizes smaller than 20 nm. As a contrast, polycrystalline silicon is a single crystalline phase with grain boundaries and the smallest crystal sizes larger than 20 nm.

With plenty of researches in the recent years, it is a common agreement that microcrystalline silicon material owns the best quality at the transition region from amorphous to crystalline (with 30% to 70% crystallinity, but strictly speaking, the term transition might be incorrect [12]). This is because the film in this region incorporates some volume fractions of crystals in amorphous networks, which have lowered light-induced degradation effect (also known as Stabler-Wronski Effect, SWE [13]) than hydrogenated amorphous silicon material but keeps reasonably high value of photosensitivity. Also, due to its amorphous nature, the absorption coefficient keeps high value.

For the formation of microcrystalline silicon, there are mainly three models related to the induction by atomic hydrogen:

1) Hydrogen etching model [14]: atomic hydrogen selectively etches away amorphous silicon.

2) Surface diffusion model [15]: exothermic recombination of atomic hydrogen on the surface locally provides sufficient energy for crystallization.

3) Chemical annealing model [16]: subsurface structural relaxation mediated by permeating atomic hydrogen gives rise to crystallization.

2.5.2 Hydrogenated Microcrystalline Silicon-Germanium Alloys

Hydrogenated microcrystalline silicon-germanium (μc-SiGe:H) alloys have been developed as a narrower variable bandgap material for multi-junction solar cells [17-18]. Due to the low absorption coefficient, μc-Si:H must be deposited about 1μm to 2μm thickness so that it can absorb enough photons. Thus, doping germanium into the microcrystalline structure is a way to elevate absorption coefficient, just like the concept of doping germanium atoms into a-Si:H network. However, alloying with germanium deteriorate the formation of crystallites and thus made the incubation layer thicker [19].

From the recent study, μc-SiGe:H get some break through about film quality by M. Kondo's group [20-21] in which they discover the film quality will only changed with germanium content in the film and the most suitable of germanium content is about 10 % to 20 %. Microcrystalline silicon germanium material with larger germanium content shown deteriorate photo response and may induce too much defects to hinder the transportation of charge carrier [22]. Moreover, other groups such as IPV also reported about the properties of μc-SiGe:H materials [23]. Until 2010, the highest reported efficiency of μc-SiGe:H single junction solar cells is 7.92 % with i-layer thickness less than 1μm [21], even higher than μc-Si:H solar cell with 2-μm-thick absorber layer. Thus, there is a great potential that the μc-SiGe:H will become the next candidate of bottom cell material.

Chapter 3 Experimental Details

3.1 Material Characterization

3.1.1 Reflection-Transmission Spectroscopy

The optical bandgap of thin film use UV/VIS/NIR spectrometers to measure transmission (T) spectra were carried out between 200 nm and 1.3 μm in the step of 2 nm. Calculating optical bandgap (E_g) has to use transmission spectra and thickness of thin film from **Eq. 3.1**.

$$\sqrt{\alpha\hbar\omega} = c(\hbar\omega - E_{opt}) \qquad \textbf{(Eq. 3.1)}$$

Fig 3.1 shows that the photo energy (ħω) as function of the $\sqrt{\alpha\hbar\omega}$. The band gap value can be determined from the expanding linear region line intercepts a-axis.

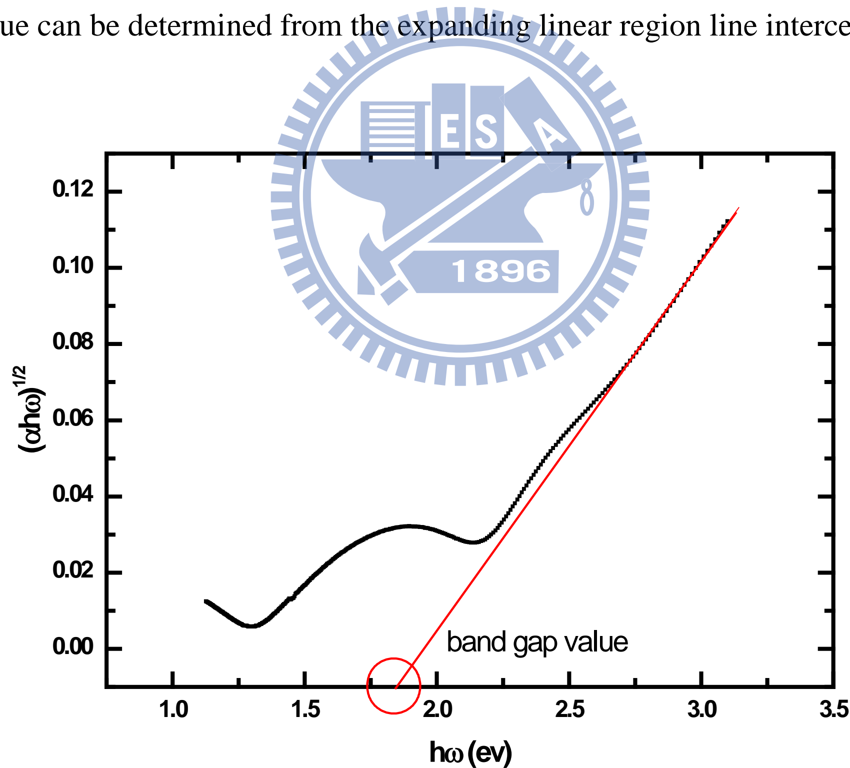

Fig 3.1 Photo energy (ħω) as function of the $\sqrt{\alpha\hbar\omega}$ and the tauc band gap

3.1.2 Raman Spectroscopy

Raman spectroscopy is the fastest and the easiest experimental technique for the

measurement of the crystallinity. The Raman scattering effect, first reported by Raman and Krishna in 1928 [24], has been used to investigate the structural property of μc-Si:H nowadays. The theory of this method is given in literature [25]. The Raman apparatus used in this study was a HORIBA, Labram HR Raman microscope with an He-Ne laser source (633 nm).

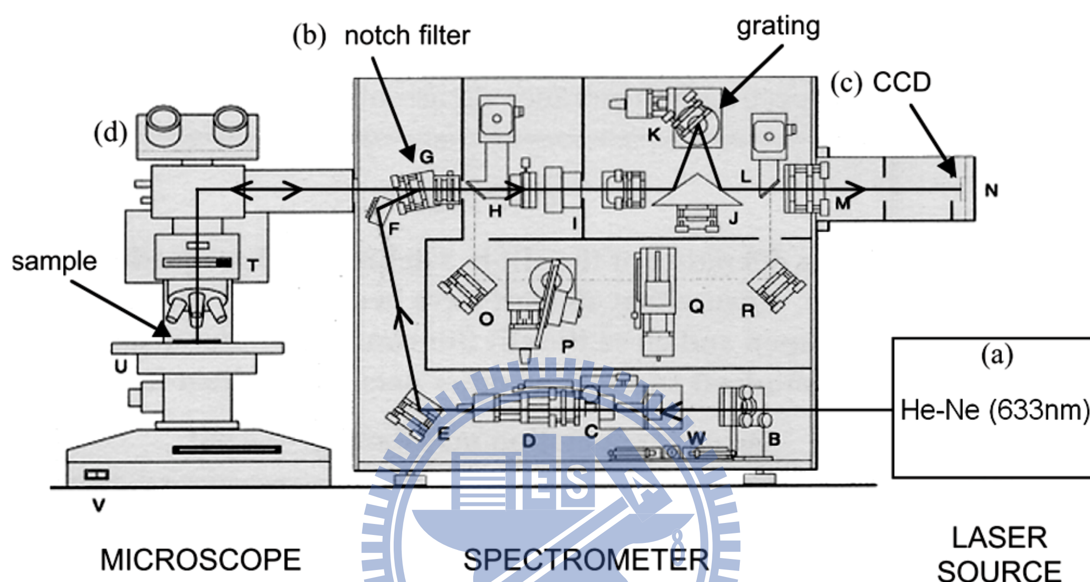

Fig 3.2 Micro-Raman spectrometer composed of an He-Ne laser source, a microscope, a notch filter, a grating and a CCD camera [26]

Fig 3.2 shows Raman spectrum of a μc-Si:H sample. In Raman spectroscopy, the signal of a-Si:H appears as a broad peak at about 480 cm^{-1}. The integrated intensity of this peak, I_a, is proportional to the volume fraction of a-Si:H in the film. The signal of microcrystalline silicon appears as a narrow peak at 520 cm^{-1}, which is the position of the transverse optic mode in mono-crystalline silicon. Another narrow peak occurs at about 510 cm^{-1} arising from the defective part of the crystalline phase (crystallites smaller than 10 nm [27], or to a silicon wurtzite phase [28] that result from twinning [29]). Therefore, the degree of crystallization can be considered proportional to the peaks at 510 cm^{-1} and 520 cm^{-1} and the **Eq. 3.2** can be obtained by the deconvolution

and integration of Raman lines. X_c is a useful factor to quantify the crystallinity of μc-Si:H thin films.

$$X_c\ (\text{crystallinity}) = \frac{I_c}{I_a + I_c} = \frac{I_{510} + I_{520}}{I_{480} + I_{510} + I_{520}} \qquad \text{(Eq. 3.2)}$$

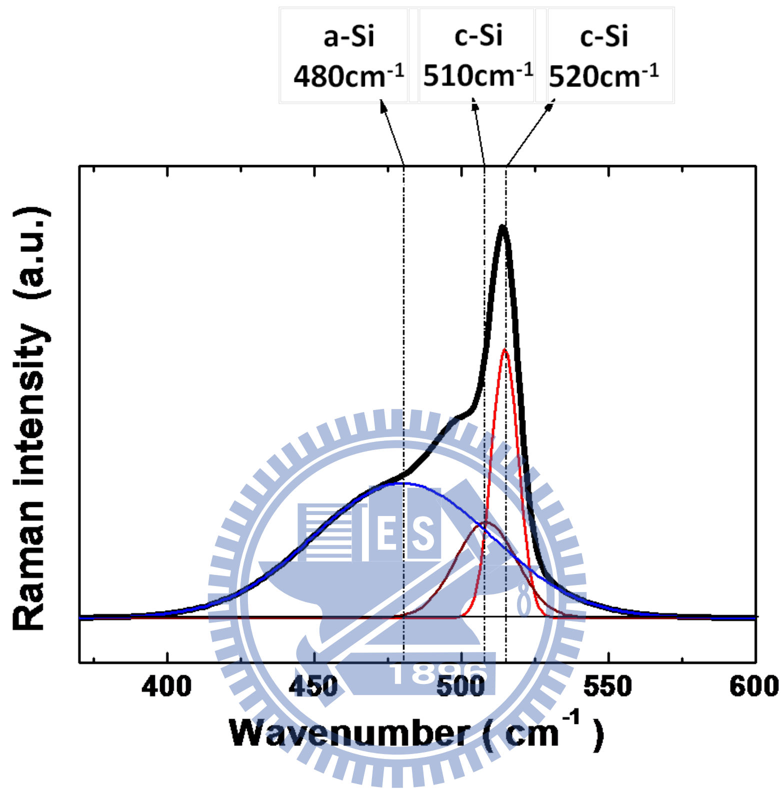

Fig 3.3 Raman spectrum of a μc-Si:H sample

3.1.3 Fourier Transform Infrared Spectroscopy (FTIR)

The incorporation of hydrogen in the amorphous silicon is beneficial because of the defect passivation. Infrared absorption spectroscopy is widely used to investigate the Si-H_x bonding configurations [30]. A peak around 2000 cm^{-1} is defined as the stretching mode of the isolated Si-H bonds, and a peak around 2090 cm^{-1} is correlated with SiH_2 and clustered $(SiH2)_n$ groups at internal surfaces of voids or grain boundries [31-32] . Different vibration frequencies for SiH_x (x=1~3) in hydrogenated amorphous

Si have been identified as shown in **Table 3.1**.

The microstructure parameter R is defined as:

$$R = \frac{I_{2090}}{I_{2000}+I_{2090}} \qquad \text{(Eq. 3.3)}$$

where I_{2000} and I_{2090} are the integrated absorption strength of the peaks at 2000 cm^{-1} and 2090 cm^{-1} respectively. The ratio R is widely used to characterize the microstructure in the a-Si:H network. As the 2100 cm^{-1} contribution increases, the ratio R increases which is the sign of poor quality material.

Table 3.1 Vibration frequencies of SiH_x (x=1~3) in a-Si:H [33]

Group	Stretching	Bending	Rocking / Wagging
SiH	2000		630
SiH_2	2090	880	630
$(SiH2)_n$	2090~2010	890,945	630
SiH_3	2014	950,860	630

3.1.4 X-Ray Diffraction (XRD)

X-Ray diffraction is a method to gain information about crystal structure, orientations and crystal defects [34] based on Bragg's equation. XRD analysis was carried out by Bede, D1 diffractometer with 2θ scan (Bragg-Brentano geometry) with an angle step of 0.1 ° and a signal collection time of 1 s. CuK_{α}–radiation characterized with a wavelength of λ=1.542Å (~8 keV) was initiated by a voltage of 40 kV and a current of 40 mA.

3.1.5 I-V Measurement

In order to investigate the conductivity of the a-$Si_{1-x}Ge_x$:H alloy, metal contacts

were deposited onto the film by thermal evaporation. Conductivity is calculated by **Eq. 3.4**, where V and I are the bias voltage and measured current, respectively. The volume of material contributing to conductivity is determined by the width (W), length (L), and thickness (t) of a cuboid located between the conducting contacts used to probe the sample in the **Fig 3.4**.

$$\sigma = \left(\frac{I}{V}\right)\left(\frac{L}{W}\right)\left(\frac{1}{t}\right) \quad \textbf{(Eq. 3.4)}$$

A prepared a-$Si_{1-x}Ge_x$:H film with silver contacts is show in **Fig 3.4**. Photoconductivity was measured by AM1.5 light spectrum with power at 100 mw/cm^2. For the amorphous silicon germanium film, the thickness is about 600 nm.

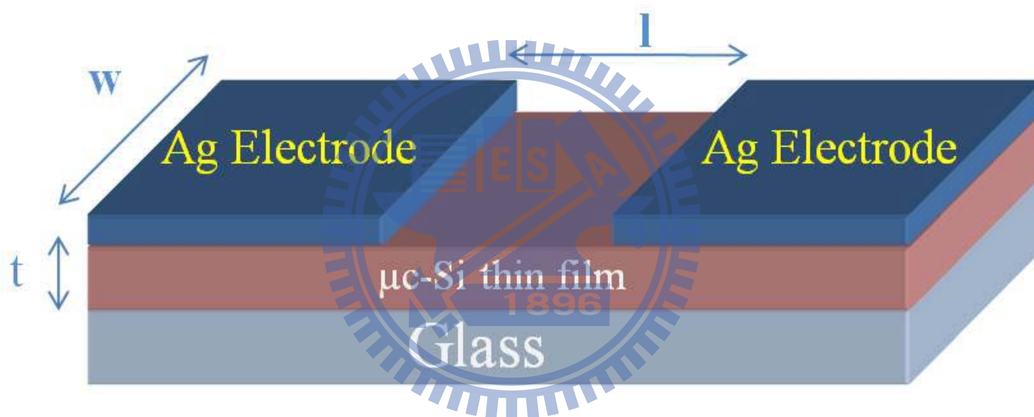

Fig 3.4 Schematics of the conductivity measurement

3.2 Solar Cell Characterization

The solar cell efficiency is measured by the solar simulator with a corrected AM 1.5 light source.

3.2.1 AM 1.5 Light Source

Solar radiation closely matches a black body radiator at 5,800 K. As the sunlight travels though the atmosphere, chemicals react with the sunlight and absorb certain

wavelengths. Perhaps the best known example is the stripping of ultraviolet light by ozone in the upper atmosphere, which drastically reduces the amount of short wavelength light reaching the Earth's surface. A more active component of this process is water vapor, which results in a wide variety of absorption bands at many wavelengths, while molecular nitrogen, oxygen and carbon dioxide add to this process. Atmospheric scattering also plays a role by removing higher frequencies from direct sunlight and scattering it about the sky. The greater the distance of atmosphere the sunlight travels through, the greater this effect, which is why the sky looks pink at sundown when the sunlight is traveling obliquely through the atmosphere.

Generally, we use the air mass (A.M.) concept to define the absorption, scattering and reflection in the atmosphere and the location and angle of solar cells. For a thickness l_o of the atmosphere, the path length l through the atmosphere for solar radiation incident at angle θ relative to the normal to the Earth's surface is

$$l = l_o / \cos\theta \qquad \textbf{(Eq. 3.5)}$$

The ratio l / l_o is the air mass coefficient, and the Attenuation by the atmosphere is

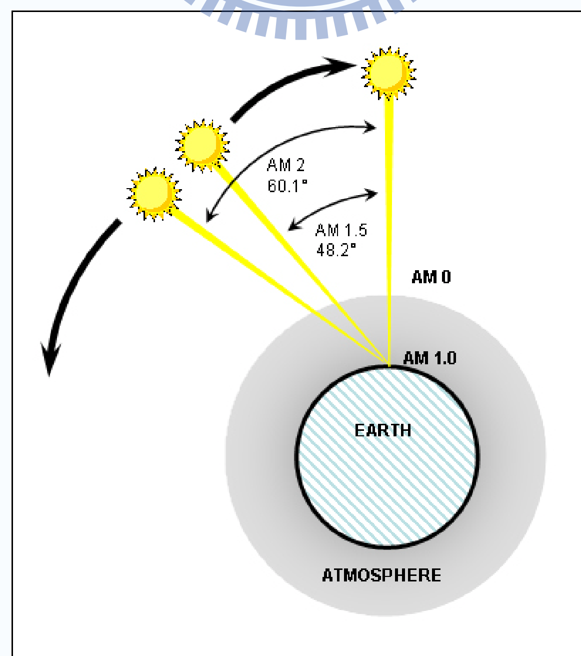

Fig 3.5 Schematic of air mass

quantified by the air mass coefficient.

As shown in **Fig 3.5**, the spectrum outside the atmosphere, the 5,800 K black body, is referred to as "AM0", meaning "zero atmospheres". Cells used for space power applications, like those on communications satellites are generally characterized using AM0.

The spectrum after traveling through the atmosphere to sea level with the sun directly overhead is referred to as "AM1". This means "one atmosphere". Conveniently, silicon solar cells are not very sensitive to the portions of the spectrum lost in the atmosphere. Since solar cell development is concentrated in the United States, Europe and Japan, an AM number representing the spectrum at mid-latitudes is much more common. "AM1.5", 1.5 atmosphere thicknesses, corresponds to a solar zenith angle of 48°, and is almost universally used to characterize solar panels.

3.2.2 Current-Voltage Characteristics

The measurement of I-V characteristics is the primary method to evaluate solar cells performance. It is measured under AM 1.5 light source.

- The efficiency (η) is defined as the ratio of the maximum power generated by the device and the radiation power incident in the area of cell.
- The short-circuit current density (J_{sc}) is the maximum current density generated by the device under light illumination.
- The open-circuit voltage (V_{oc}) is the maximum voltage generated by the device under light illumination.
- The fill factor (F.F.) is defined as a ratio of maximum power generated by the cell and the ideal power generated which is equal to $I_{sc} \times V_{oc}$. This factor relate to the shunt resistance, series resistance and material quality in the device.

3.2.3 Quantum Efficiency

Spectral response provides the information about the working principle of solar cell. The Quantum efficiency is defined as

$$\mathbf{Q.E.} = \frac{\mathbf{J_{ph}(\lambda)}}{\mathbf{e \times \varphi\,(\lambda)}} \qquad \textbf{(Eq. 3.6)}$$

where, J_{ph} is the photo-generated current density per wavelength interval, e is the elementary charge, and ψ is the number of photon per time, area, wavelength interval. Therefore, the quantum efficiency describes the probability that an incident photon generates a charge carrier pair which contributes to the photo current.

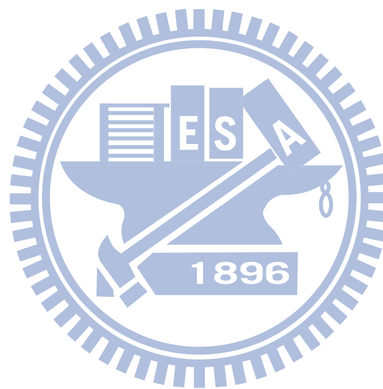

Chapter 4 Results and Discussions

4.1 Deposition and Characterization of a-SiGe Thin-Films

Hydrogenated amorphous silicon germanium and Hydrogenated microcrystalline silicon germanium were deposited using SiH_4, GeH_4 and H_2 by radio frequency (27.12 MHz) plasma enhanced chemical vapor deposition (PECVD) system. Doping layers were prepared by using diluted B_2H_6 or PH_3 with SiH_4 and H_2. Prior to depositing all the samples, NF_3 and Ar were introduced to clean the chamber. Corning Eagle2000 glass and c-Si wafer substrate were cleaned by KG detergent and RCA standard cleaning process, respectively. All the samples were deposited after a background pressure of $5 * 10^{-4}$ Pa was reached. In this study, a-SiGe:H and μc-SiGe:H alloys were prepared on 5cm x 5cm Corning Eagle 2000 glasses and 1.5cm x 1.5cm c-Si wafers. The films grew on glass substrate were used to analyze optoelectronic properties, and the films grew on c-Si wafer were used to determine the hydrogen bonding configuration by FTIR.

4.1.1 The Effect of Hydrogen Dilution on Deposition Rate and Film Quality

Fig 4.1 (a) shows that the deposition rate drops drastically with increasing hydrogen dilution ratio at different GeH_4 concentrations. This is because hydrogen radicals on the growing surface will enhance the etching effect. Hydrogen radicals will selectively break the weak Si-Si bond and leave a vacancy to give a chance to form a stronger bonding. Also, the concentration of SiH_4 and GeH_4 in H_2 were lower

with increasing hydrogen dilution ratio. The deposition rate at different GeH4 concentration, however, shows no significant variation.

Fig 4.1 (b) shows the microstructure factors calculated by the signal of Si-H and Si-H_2 bonding configuration obtained from FTIR. The figure shows that when hydrogen dilution ratio increases, the SiH_2/SiH ratio drop and then may slightly rise again. This indicates that hydrogen etching effect will improve film quality, but too much hydrogen will deteriorate the film quality. Furthermore, films deposited by higher GeH_4 concentration will result in higher SiH_2/SiH ratio. This is due to the films incorporated with more Ge atoms will deteriorate the film quality.

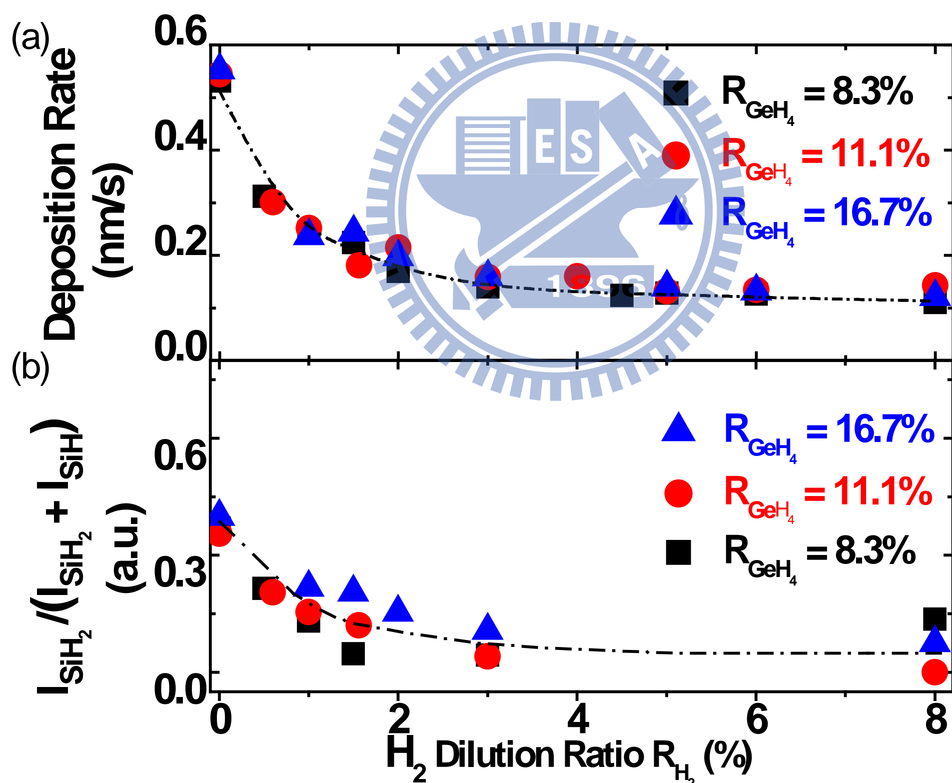

Fig 4.1 **(a) The deposition rate and (b) the bonding intensity ratio as a function of R_{H2} at different R_{GeH4} at 8.3 %, 11.1 % and 16.7%, respectively**

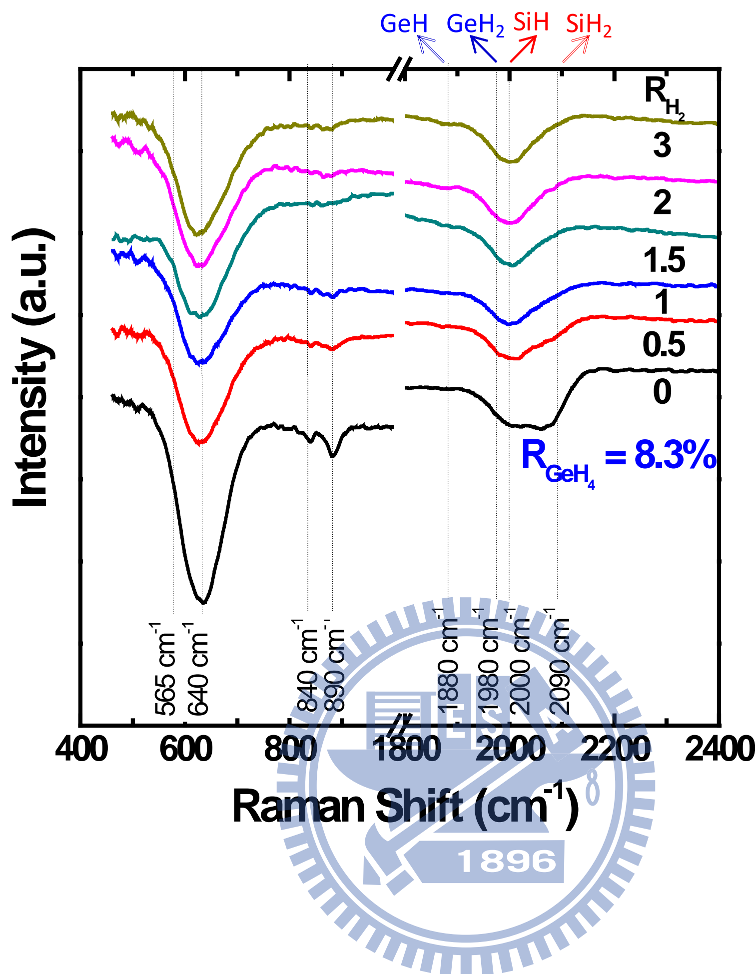

Fig 4.2 **Fourier transform infrared spectra of a-$Si_{1-x}Ge_x$:H alloys with different R_{H2} at R_{GeH4} = 8.3%**

4.1.2 The Effect of Hydrogen Dilution on Conductivity Properties

Fig 4.3 shows that when hydrogen dilution ratio increased, the conductivities raise about one order of magnitude, and the photo response increased, too. This should be due to the increasing of hydrogen etching ability which makes film quality become better. But the film quality gets worse when hydrogen dilution exceed a threshold value. This may be due to the severe gas phase reaction or the over etching, which produces more defects in the film and deteriorates film quality.

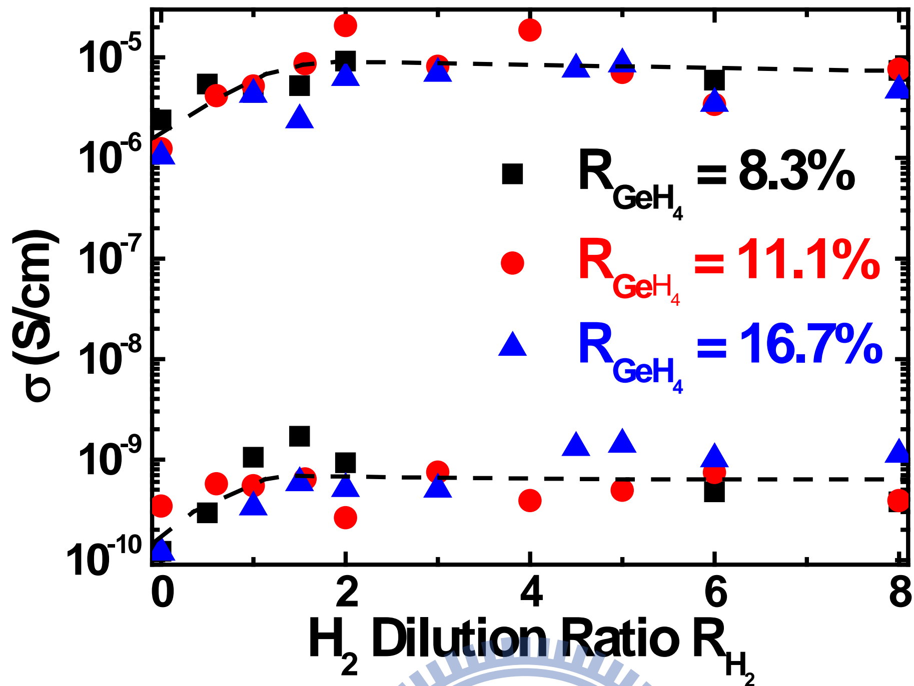

Fig 4.3 The dependence of R_{H2} on photo-conductivity and dark-conductivity of a-$Si_{1-x}Ge_x$:H alloys at three R_{GeH4}

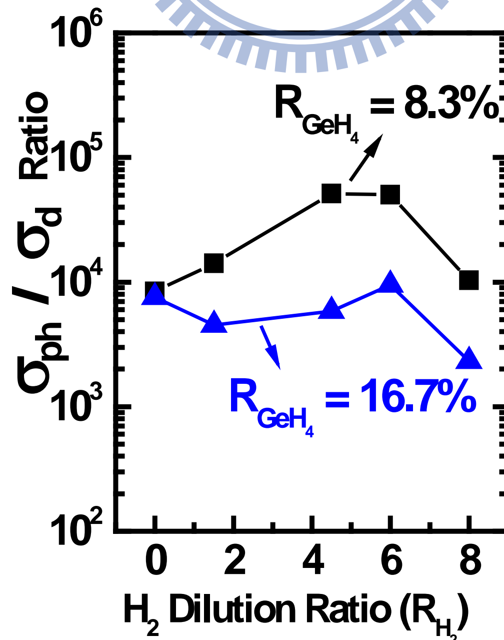

Fig 4.4 Dependence of the photo-to-dark conductivity ratio with hydrogen dilution ratio.

4.1.3 The Effect of Hydrogen Dilution on Optical Bandgap and Ge Atomic Concentration

Fig 4.5 and **Fig 4.6** show that the relationship between hydrogen dilution and the Ge content and also the bandgap. When we increase the hydrogen dilution the germanium content will also increase due to the more efficient dissociation of GeH_4 than SiH_4. This can be seen from the three GeH_4 concentrations. Also, the incorporation of Ge atom into the film will lower the bandgap of the material so that we can manipulate the bandgap of SiGe alloy by control the amount of hydrogen dilution, which is shown in **Fig 4.5**. There is another thing shown from **Fig 4.5** that

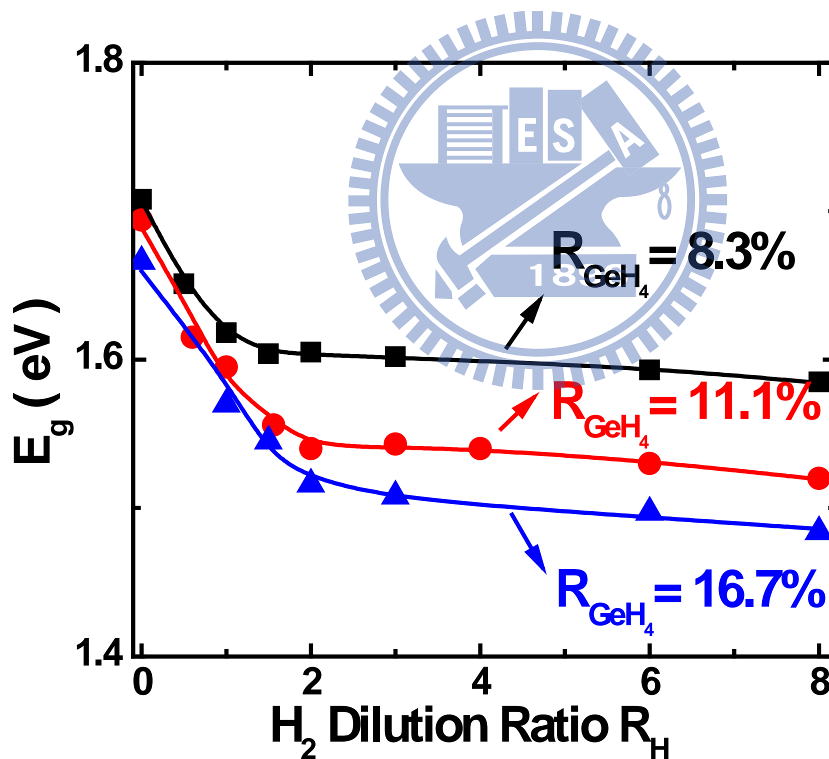

Fig 4.5 The dependence of optical band gap of a-$Si_{1-x}Ge_x$:H alloys on R_{H2} at various R_{GeH4}

the bandgap drops drastically when hydrogen dilution between 0 and 2 and then

reaches a saturation value for three different GeH_4 concentrations. **Fig 4.7** shows another effect that as hydrogen dilution increase the H content in the film decreased, which arise from the hydrogen facilitates the dissociation of GeH_4 and strengthens the hydrogen etching effect so that the Ge content is increased while H content is decreased.

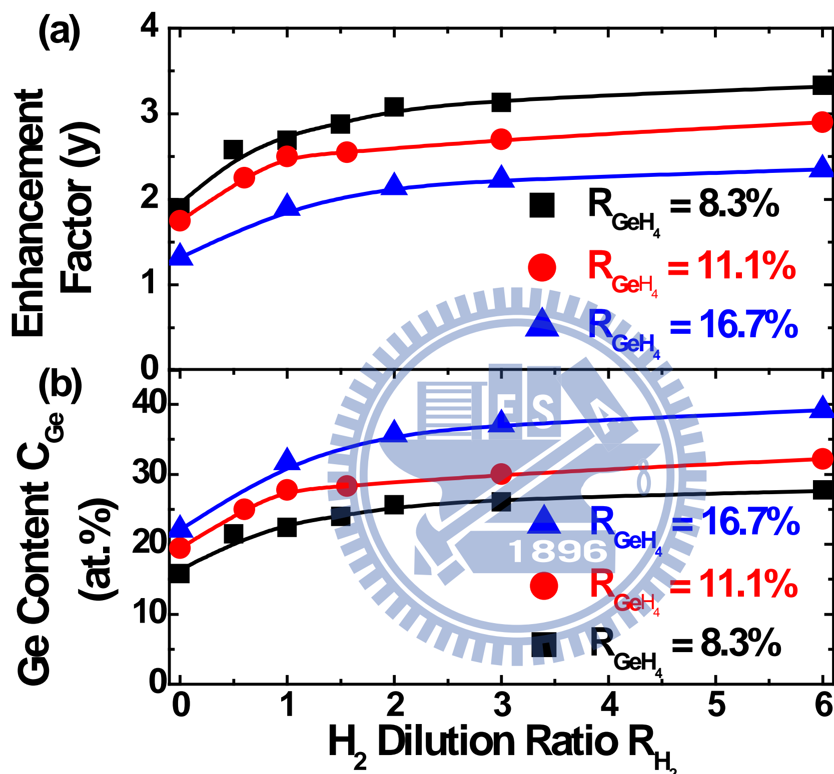

Fig 4.6 (a) Enhancement factor and (b) Ge content in a-$Si_{1-x}Ge_x$:H alloys as a function of R_{H2} for three R_{GeH4} at 8.3 %, 11.1 % and 16.7 %, respectively.

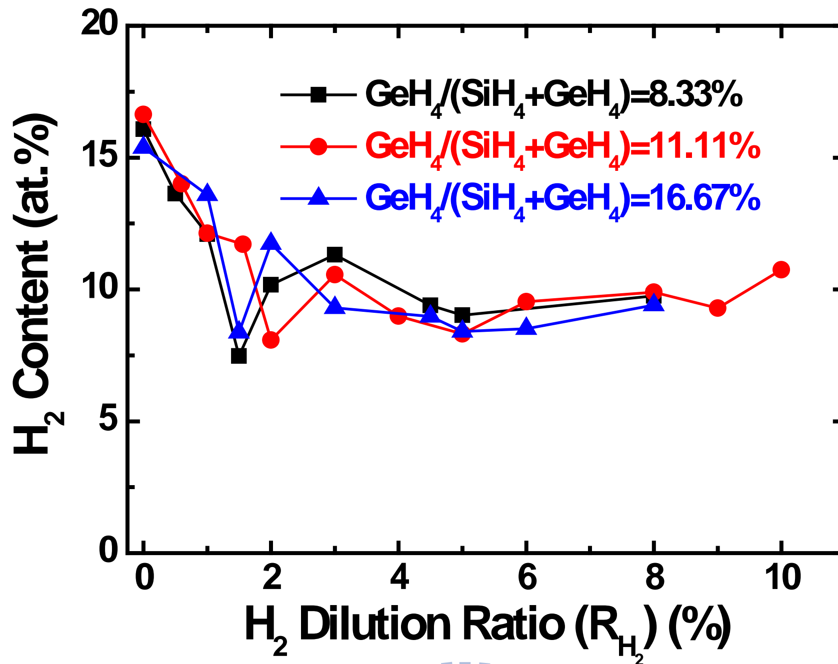

Fig 4.7 Hydrogen content as a function of hydrogen dilution ratio at different germane concentrations.

ES A 1896

4.1.4 The Effect of RF Power on Conductivity

From **Fig 4.8**, the increase of rf power makes the photo conductivity rise and dark conductivity decrease. Also, the figure shows the same trend as above mentioned that when hydrogen dilution increase the deposition rate and bandgap decrease and reach a saturation region. The figure at bottom shows that the influence of hydrogen dilution to SiH_2/SiH, GeH_2/GeH ratio and power. As hydrogen dilution increase the SiH_2/SiH, GeH_2/GeH ratio drop because hydrogen radicals will etch the growing surface and also feed energy to make atoms find a binding site with lowest potential energy. Moreover, increase power can lower the SiH_2/SiH and GeH_2/GeH ratio this can be explained by that it gives more energy to let atom diffuse on the growing surface and find a lowest energy binding site.

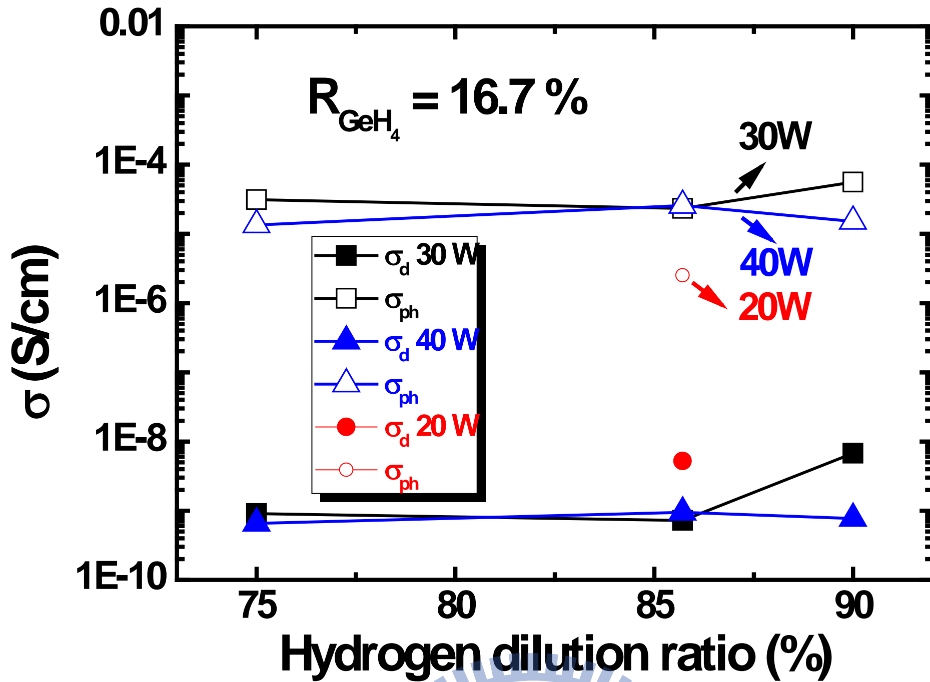

Fig 4.8 Dependence of the photo-conductivity (σ_{ph}) and dark-conductivity (σ_d) with hydrogen dilution ratio

4.2 a-SiGe:H Single Junction Solar Cell Optimization

Although we have made certain progress in cell performance, there are still some aspects needed to be improved for higher efficiency. Therefore, in this section, the improvement of a-SiGe single junction solar cell from a baseline to the latest result will be discussed. Besides, some possible issues that can cause efficiency improvement will also be disclosed here.

4.2.1 Effect of Buffer Layer on Cell performance

In this section, we replace original a-Si p-layer with undoped a-Si buffer layer and hypothesize that this change will increase J_{SC} and FF. Then further increasing germane concentration in gas phase from 11.1 % to 16.7 %, the characterized Ge content by XPS

shows that the film deposited at 16.7% R_{GeH_4} is composed of about 38 % Ge atom and bandgap is 1.45 eV by Tauc plot [35].

From the former structure, the thin a-Si p-layer between a-Si p+ and a-SiGe i-layer formed a graded bandgap profiling, but doping boron also induce a large amount of defects in a-Si:H material; furthermore, when depositing i-layer, the substrate heating will provide enough energy to let boron diffuse into a-SiGe i-layer and decrease film quality. Therefore, inserting a buffer layer into p/i interface can resist boron diffusion and can eliminate the defects induced by doping boron which in turn improve the interface quality. Furthermore, the a-Si n-layer between i-layer and n+ layer may hinder charge carrier transport as well. So, by considering above, we made following two changes:

1. Replace a-Si p-layer with a-Si buffer layer
2. Replace both a-Si p-layer and a-Si n-layer with a-Si buffer layer.

Fig 4.9 shows the I-V curve comparison between cells with one p-layer replaced by a buffer layer and two buffer layer replaced. Solar cells represent here were not post annealed. Cell structure with two buffer layers insertion is higher in efficiency than the cell with one buffer layer insertion due to the improved J_{SC} and FF. Moreover, the short circuit current density and therefore efficiency is higher than former structure, which can be explained by the improved interface quality by lowering the defect density and prevention of impurity diffusion. So we can conclude that cell with structure p+/b/i/b/n+ will present better cell performance than the former structure p+/p/i/n/n+.

Another interesting observation can be seen from **Fig 4.10** is that quantum efficiency had been improved compared with the former one by the increased absorption in the whole spectrum. However, the absorption range still has no significant shift toward long wavelength region; despite that germanium content in the

film is about 38 %. The results conflict the general understanding that elevated germanium content will directly increase the absorption of long-wavelength region. The reason for below expectation absorption in long wavelength region is still not clear, and the possible reason maybe the diffusion length is shortened by the increased germanium content, so that the charge carrier excited by long wavelength photons will have larger chance to be recombined before collected by external circuit. So, if the hypothesis is correct, then further optimization of film thickness is needed for improvement of quantum efficiency, and other possible solutions are now under consideration.

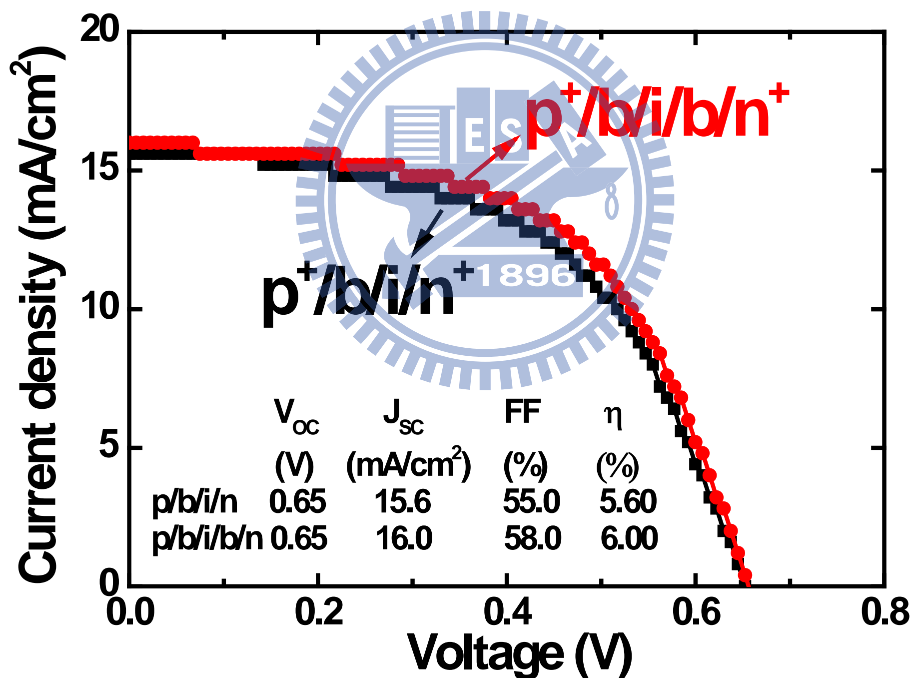

Fig 4.9 Illuminated J-V characteristics of 216-nm-thick a-$Si_{1-x}Ge_x$:H single junction solar cells prepared with one or two buffer layer.

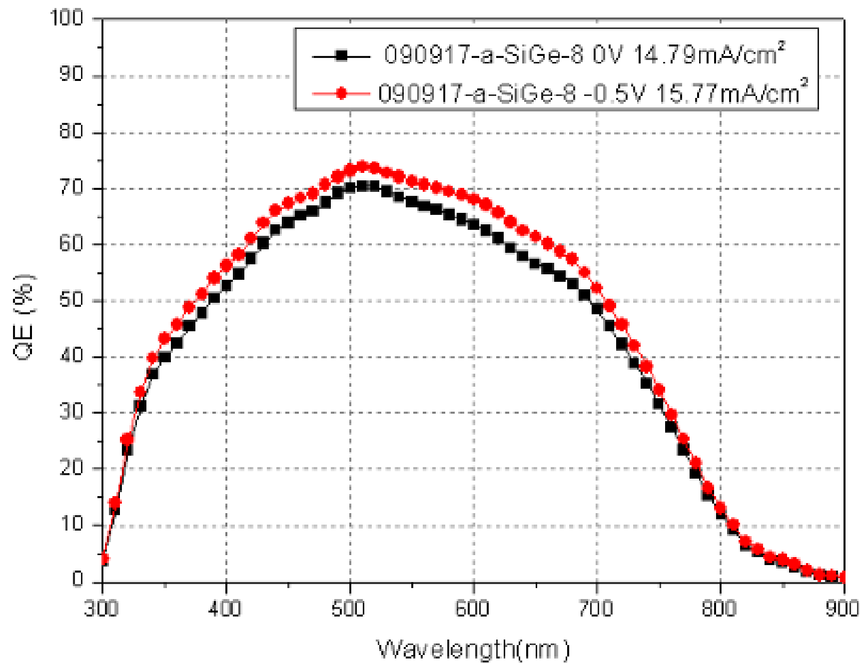

Fig 4.10 QE spectra of a 216-nm-thick a-$Si_{1-x}Ge_x$:H single junction solar cell under zero bias and -0.5 V bias.

4.2.2 RF Power Effect on cell performance

Remind that post-annealing will provide some energy to vibrate molecule and ease tension within material, increasing RF power also provide energy for molecule rearrangement. When depositing thin film, the dynamic balance is very important, for material relax itself while atom continuously deposit on growing surface. This process is more efficient compared with post-annealing. Therefore, elevate RF power will facilitate molecule diffusion on the growing surface and speed the deposition rate. Theoretically, higher RF power will improve film structure, but it also increase deposition rate so that the molecule might have no chance to diffuse due to the fast growth on growing surface. So, the preferable power is the result of dynamic balance between molecule relaxation and deposition rate.

Recall from previous result in **Fig 4.8**, when we elevate power from 20 W to 30 W, both photo and dark conductivity were improved nearly one order, as expected

with pervious discussion. But we notice one interesting thing from **Fig 4.11** that cell with a-SiGe i-layer deposited at 20W has higher efficiency than cell deposited at 30 W. This observation can be understood by that although increasing RF power will facilitate film relaxation, but the film deposited at 30 W will suffer from stronger ion bombardment than film deposited at 20 W, thus create more defect throughout the material. And in turn lower the FF at higher power. So, we can conclude that the film quality is result of compromise of dynamic situation. Further optimization between 20 W and 30 W should be done in the future.

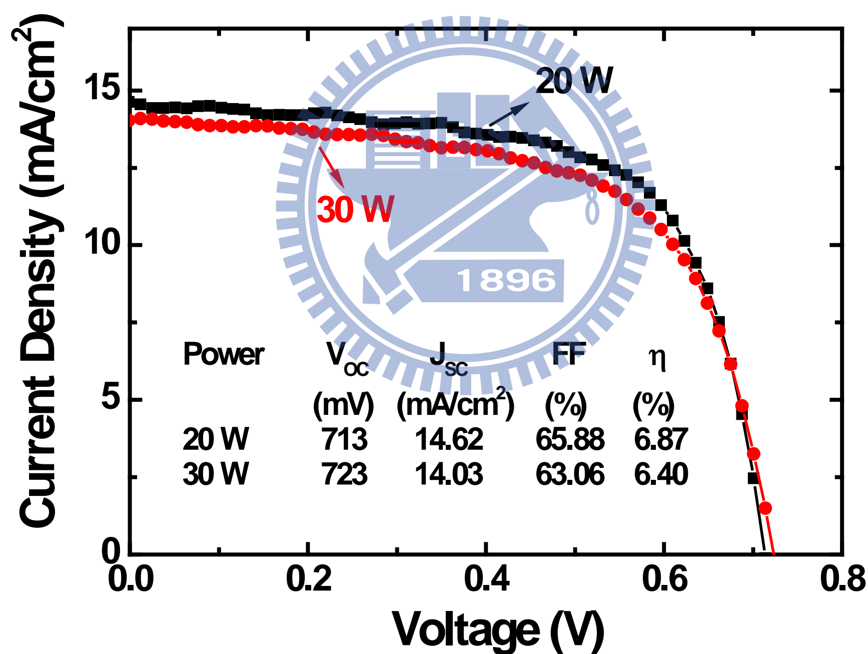

Fig 4.11 Illuminated J-V characteristics of a-$Si_{1-x}Ge_x$:H single junction solar cells with i layer prepared with 20 W and 30 W.

4.2.3 Thickness Variation for p+/b/i/b/n+ Structure

In this section we want to further optimize i-layer thickness because we elevate germane concentration from previous 11.1 % to now 14.3 %, so that the proper film

thickness will change. Recall that in section 3.2.2 we have mentioned that the optimized thickness will change with Ge content in the film and also found that i-layer thickness of 200 nm will represent best cell performance for germanium concentration 11.11% in gas phase. Another difference from sec. 3.2.2 is structure, the former baseline is p+/p/i/n/n+, while after a serious experiments we found p+/b/i/b/n+ will represent better cell performance. Hence the proper i-layer thickness should be find out again.

The comparison of I-V curve between different i-layer thickness 180 nm and 226 nm are shown in **Fig 4.12**, and cell with thinner i-layer thickness present lower efficiency than cell with 226 nm thickness. Although shorten the i-layer thickness makes J_{SC} become larger, but FF drops and compensate the increase of J_{SC}, so total efficiency is lower than thicker i-layer thickness. The reason of this result is not so clear because when thickness is thinned, charge carriers has higher possibility to be separated from the material before being recombined, which in turn cause larger J_{SC}. However, the drop of FF is unexpected and might be an experimental error. Therefore, further examine of film thickness is needed to find out an optimal thickness.

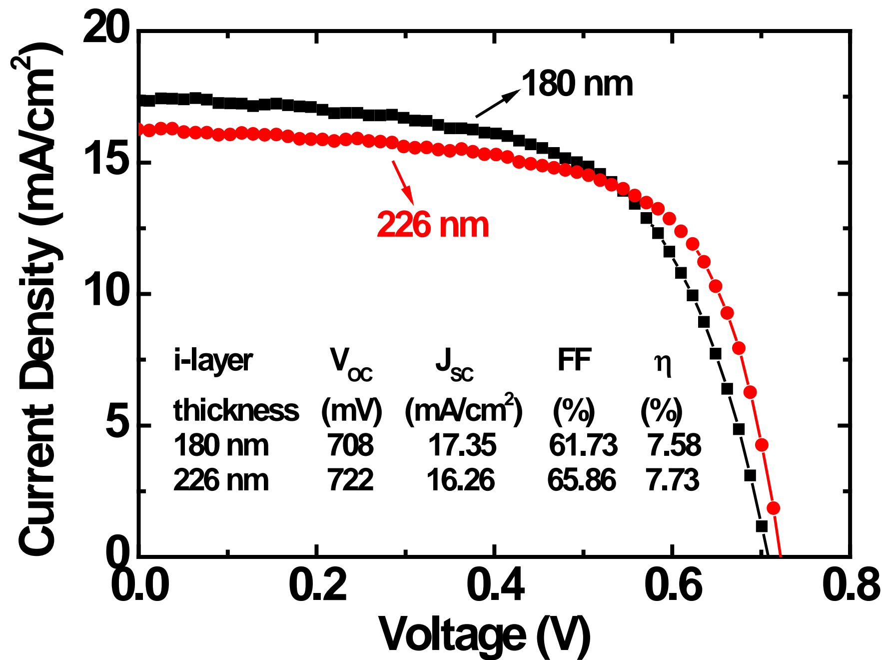

Fig 4.12 Illuminated J-V characteristics of a-$Si_{1-x}Ge_x$:H single junction solar cells with different i layer thickness (180 nm and 226 nm).

4.2.4 Layer Thickness Variation with Elevated Ge Incorporation

In order to increase the ability to absorb more long-wavelength photons, the germane concentration in gas phase increased from 8.3% to 11.1%, and then evaluated the effect of i-layer thickness on cell performance. As shown in **Fig 4.13** and **Fig 4.14**, cell with 200 nm i-layer thickness presents better cell performance compared with 150 nm and 300 nm ones. The main difference between these cells is J_{SC}, which can be explained by increased absorption in infrared region and diffusion length. As thickness vary from 150 nm to 200 nm, the current density increased due to the improved absorption of infrared photons. However, when film thickness vary from 200 nm to 300 nm, despite that the further increase in infrared photon absorption, FF decrease due to film thickness exceed the diffusion length of a-SiGe material and result in poor charge carrier transport. Therefore, the proper i-layer thickness in this experiment should be

200 nm and the proper thickness will change with the germanium content in the film. In the following experiment, we will fix i-layer thickness around 200 nm for further increased in Ge content and then find tune i-layer thickness again to find out a more suitable thickness.

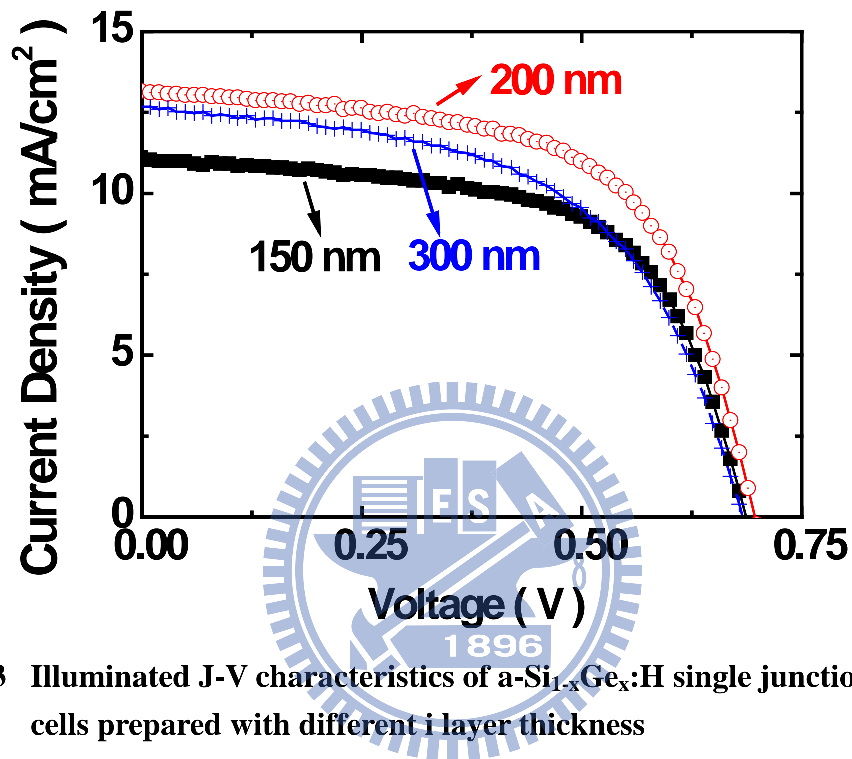

Fig 4.13 Illuminated J-V characteristics of a-$Si_{1-x}Ge_x$:H single junction solar cells prepared with different i layer thickness

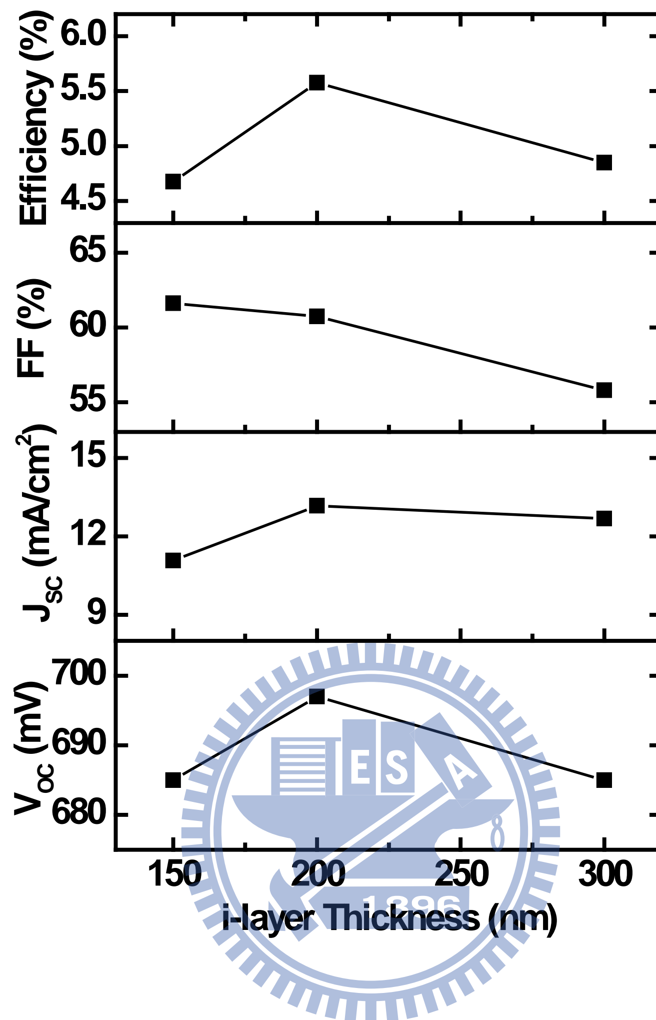

Fig 4.14 Dependence of V_{OC}, J_{SC}, FF and Efficiency of a-$Si_{1-x}Ge_x$:H single junction solar cells on i layer thickness.

4.2.5 Back Contact Comparison

Back contact act as an electrode and also a light trapping structure, proper surface microstructure together with front TCO light trapping structure can increase effective optical path length by several times. TCO back contact can be sputtered on the top of n-layer and provide resistive ability to post-oxidation.

Thus, we examine three kinds of back contact: directly coat Ag onto semiconductor, ITO coated with Ag electrode and ZnO coated with Ag electrode, the

result is shown in **Fig 4.15**. As we can see from the figure, cell with n-layer coated with TCO and Ag electrode will represent higher J_{SC} and also FF than Ag electrode only, due to the better charge carrier collection ability by TCO. Another thing shown in the figure

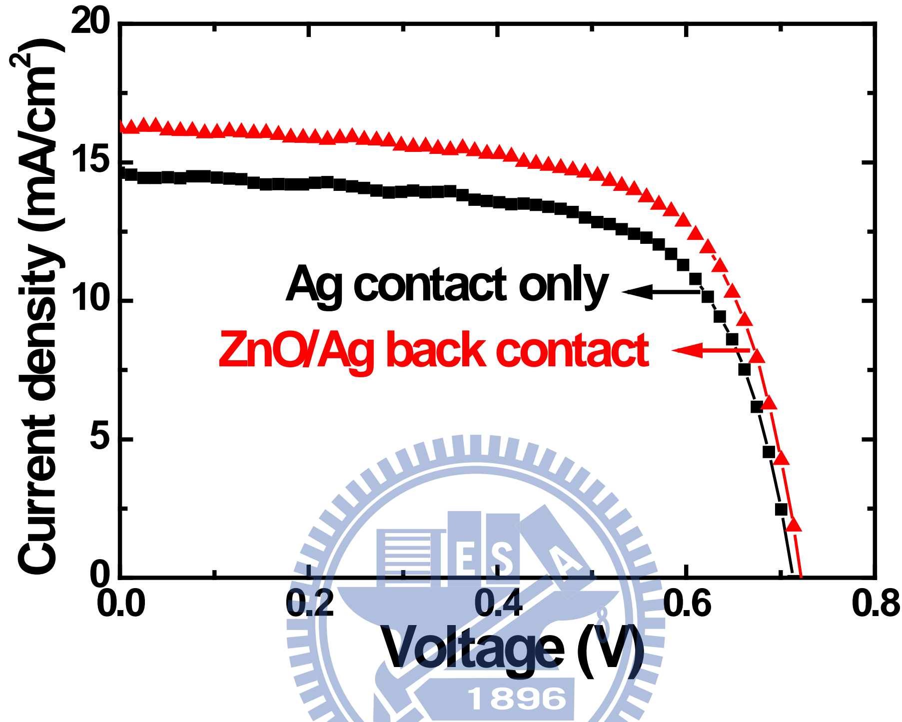

Fig 4.15 Illuminated J-V characteristics of 216-nm-thick a-$Si_{1-x}Ge_x$:H single junction solar cells with different combination of back contact material.

Table 4.1 Illuminated J-V parameters of a-$Si_{1-x}Ge_x$:H single junction solar cells with different combination of back contact material.

	V_{OC} (mV)	J_{SC} (mA/cm2)	FF (%)	Efficiency (%)
Only Ag contact	713	14.62	65.88	6.87
ZnO/Ag back contact	722	16.26	65.86	7.69

is that ZnO back contact is better than ITO in our experiment, so that we will choose ZnO as back contact for current research. Further improvement of TCO is now under

investigation.

4.2.6 Anneal Temperature Optimization

In the cell fabrication, post-annealing is also an essential part of standard cell fabrication process. But in the thin film characterization, material suffer from post-oxidation will certainly decrease film quality especially in microcrystalline based material [36], because the incorporated impurities such as oxygen atom served as a dopant that will contribute electron to rise dark conductivity and also create more defect lead to deteriorate film quality. Hence, post-annealing is not preferable for thin film characterization.

Apart from thin film characterization, post-annealing of cell covered by back contact will not deteriorate the cell performance; on the contrary, under proper post-annealing condition, cell performance will be greatly improved by providing extra energy to relax tension within not adequately bonded atoms and improve atoms arrangement. Finally, post-annealing provides a better interface contact between cell and material. Furthermore, the annealing condition will differ slightly from material to material. Therefore, we should test annealing condition before further investigation of cell performance.

Fig 4.16 and **Fig 4.17** show the relationship between different annealing temperatures on cell performance lasting for 30 minutes with pump fully open. We can observe that when annealing at 155 ^{O}C (actual value), the cell reaches its maximum efficiency; however, further increase annealing temperature will deteriorate cell efficiency drastically. So the proper annealing temperature should be around 150 ^{O}C to

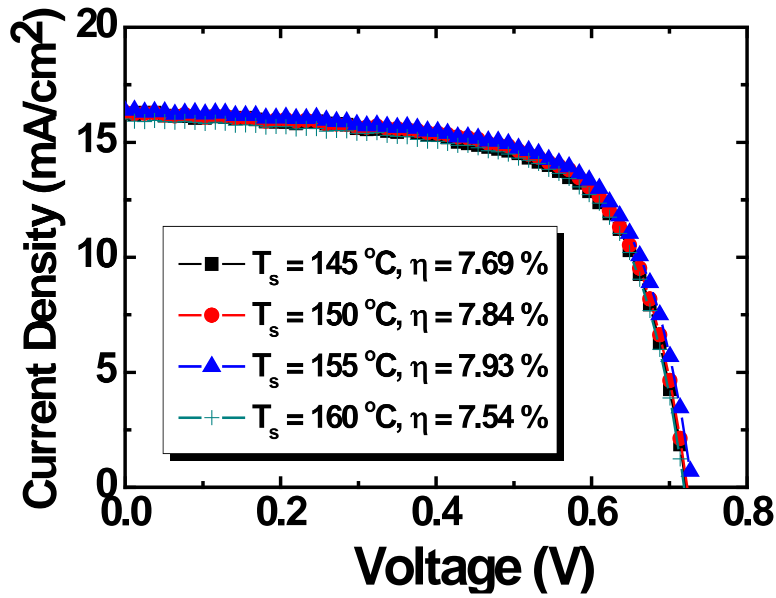

Fig 4.16 Illuminated J-V characteristics of 216-nm-thick a-$Si_{1-x}Ge_x$:H single junction solar cells post-annealed at various temperature (T_S= 145 ^{O}C, 150 ^{O}C, 155 ^{O}C, 160 ^{O}C).

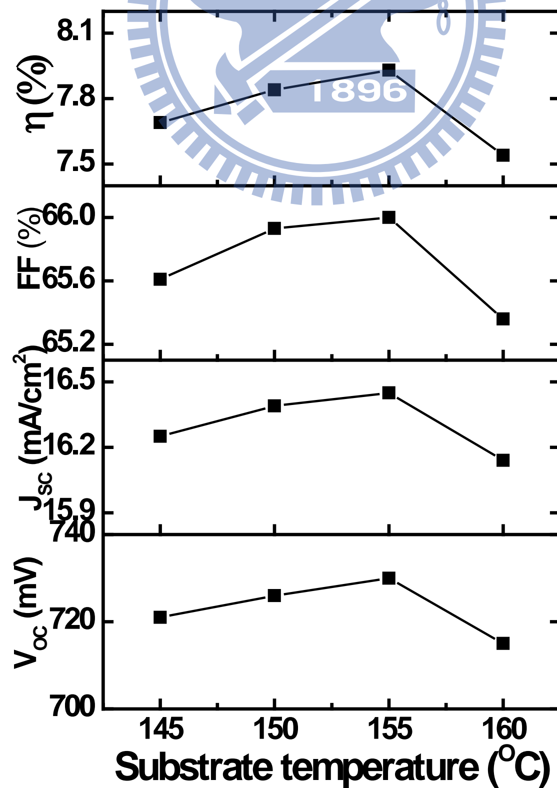

Fig 4.17 Dependence of V_{OC}, J_{SC}, FF and Efficiency of a 216-nm-thick a-$Si_{1-x}Ge_x$:H single junction solar cell on post-annealing temperature.

achieve maximum cell efficiency and avoid suddenly dropping in cell efficiency. This temperature is also examined by other cells and cell maximum efficiency shows agreement with annealing temperature about 150 ^{O}C. So, in the following experiment we will set anneal temperature at 150 ^{O}C to ensure cell efficiency and maintain consistency.

4.2.7 Bandgap Engineering

From previous discussion, our cell structure and deposition condition had been changed a lot. The current structure is p+/b/i/b/n+ and p+-layer is a-Si p-layer. Intrinsic layer thickness is 226 nm. According to literature about a-SiGe […],bandgap profiling in intrinsic layer is an essential part to achieve higher cell efficiency and better stability (thickness can be thinner).

Due to the doping of germanium atom, the bandgap of a-SiGe material can be easily tuned by control germanium content in film, which provide a chanceto smooth the band gap. As we know, bandgap discontinuity is a problem is narrow bandgap material such as a-SiGe, charge carrier will be hard to transport through bandgap discontinuity site thus lower short circuit current. Therefore, if we dynamically change germane concentration (or stepwise change) in gas phase when deposition, we will have a gradually narrow and then become larger bandgap. Smooth bandgap will help charge carrier transport easily and also increase V_{OC}. Moreover, a gradual change of bandgap near n-layer can facilitate hole transport due to the smaller mobility of holes. In pratical situation, there are a lot of possible bandgap profiling, and by the help of computer modeling, we conclude that the “V” shape will have best efficiency. The bandgap profiling used in our device is decreasing from about 1.75 eV to 1.53 eV near

p-layer, and then fix at 1.53 eV, finally gradually magnify the bandgap. Also note that the slope of bandgap changing of two sides are different, the slope is sharp near p-layer while the slope is smooth near n-layer. This is because the hole needs gradual change in bandgap to help them transport, while the sharp change near p-layer will give larger bandgap and V_{OC}, too.

Fig 4.18 illustrates the improvement of FF by bandgap grading. We change germanium content in film by stepwise change germane concentration in gas phase. Although the step is not so smooth but the result still coincident with our expectation, graded bandgap increased cell efficiency by enhancing FF and V_{OC}. This is because the improved charge carrier transport by bandgap profiling and also cause larger V_{OC}. After knowing that, we will further optimize the bandgap grading structure.

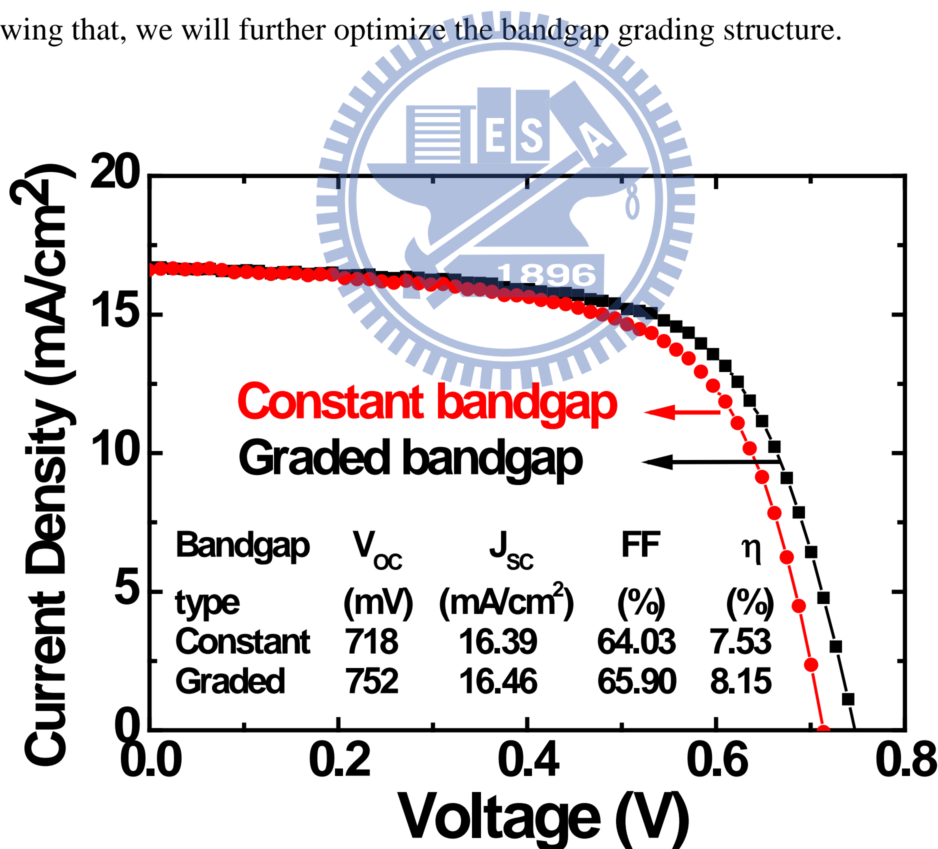

Fig 4.18 Illuminated J-V characteristics of a-$Si_{1-x}Ge_x$:H single junction solar cells prepared with constant and graded GeH_4 concentration.

4.2.8 n-layer Thickness Variation

The last part we examine the influence of n-layer thickness to device quality. As we can see from the **Fig 4.19**, the n-layer thickness is changed from 30 nm to 20 nm, and the cell efficiency has been greatly improved due mainly to elevated FF. Thus, the possible reason might be the decrease of resistance by decreasing n-layer, and we can get an idea from this figure that n-layer thickness will have impact on the device quality. Therefore, more tests should be done to examine the optimal thickness of n-layer.

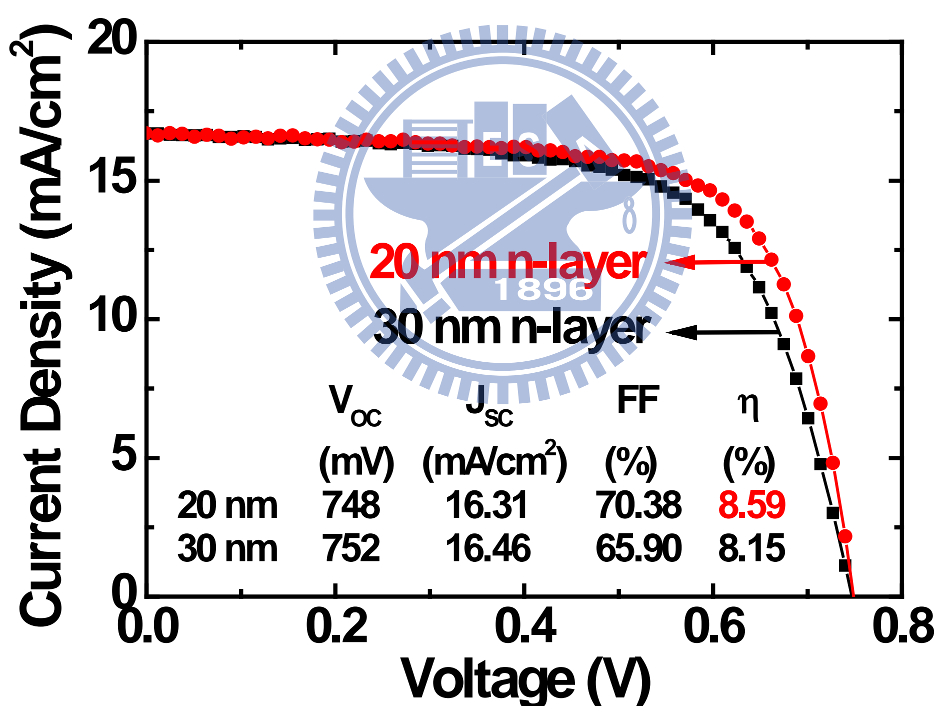

Fig 4.19 Illuminated J-V characteristics of a-$Si_{1-x}Ge_x$:H single junction solar cells prepared with constant and different graded GeH_4 concentrations.

4.3 Deposition of μc-SiGe:H Thin-Film and Performance of Solar Cells

From literature we know that microcrystalline silicon material grows near the amorphous to microcrystalline transition will have better film quality. To grow film near the transition we have some options to do, such as changing RF power, changing hydrogen dilution. Also, the amount of atomic germanium in the film plays an important role to film quality. In the following paragraph we discuss three factors mentioned above that will influence the crystallinity respectively.

4.3.1 Effect of RF Power on Film Quality

From **Fig 4.20** we can see that as the power increases the silicon crystalline peak appears and then reaches saturation region after 200 W. We also notice that when power varying from 100 W to 200 W, the transition from amorphous to microcrystalline appears. We can compare the Raman spectra to conductivity (**Fig 4.21**). When varying power from 200 W to 600 W, the crystallinity reaching a saturation region so that the conductivity become almost the same. Also, the dark conductivity is about 10^{-6} order which means that the film is highly crystallized. But when power varying from 100 W to 200 W (more specifically from 100 W to 130 W), a distinct change appear so we can conclude that the film deposited at 130 W is suitable for a microcrystalline silicon germanium film. Note that when depositing film at 130 W and 160 W there are some powder formed, which is not favorable for deposition. Some group observes the same phenomenon that powder formation when film depositing nearing the transition region. So we will fix power at 200 W and try to

changing hydrogen dilution to let the film deposit closer to the transition region.

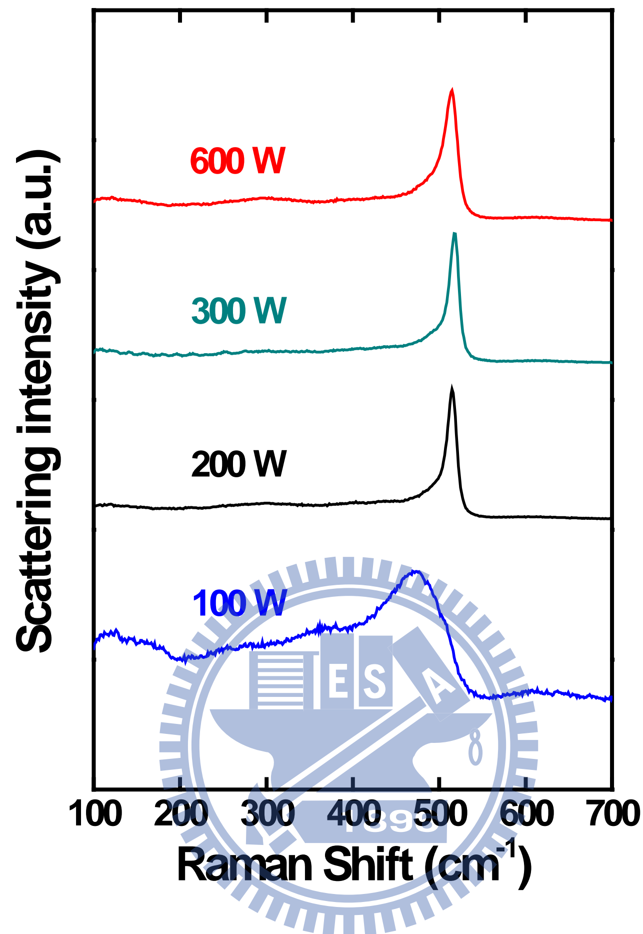

Fig 4.20 Raman scattering spectra for μc-$Si_{1-x}Ge_x$ films deposited on bare glass at fixed germane concentration (R_{GeH_4}) with various power ranging from 100 W to 600 W.

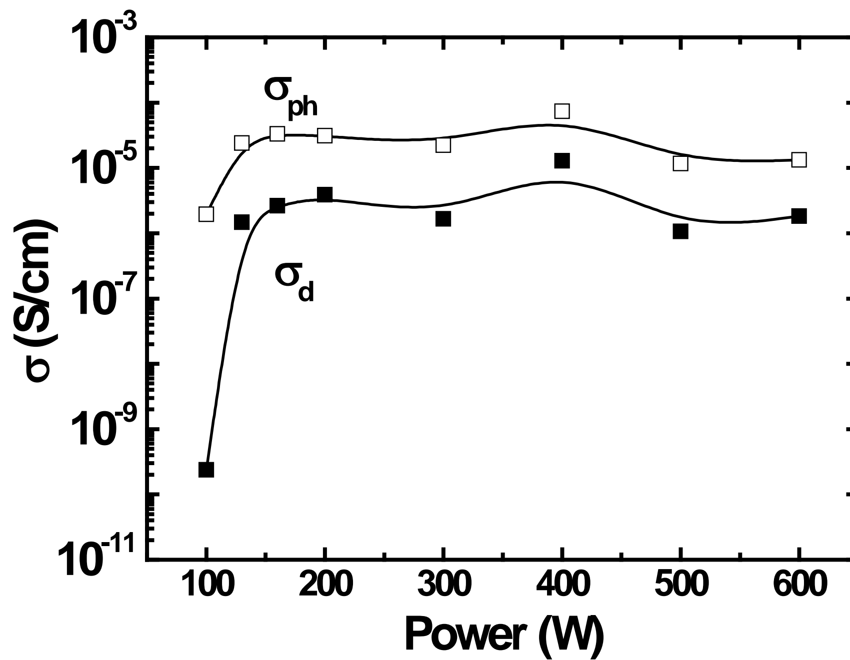

Fig 4.21 Dark conductivities (solid symbols) and photo conductivities (open symbols) as a function of discharge power.

Also, we can observe from **Fig 4.22**, the (220) direction is more pronounced as film deposited closer to the transition region so as to grain size. Note that the (220) crystallization direction is perpendicular to the growing surface, and the charge carrier in solar cell also transport in the direction perpendicular to the growing surface. So the (220) direction will be helpful to charge carrier transport. That is one of the reason that when film deposit at transition region will get better film quality.

1896

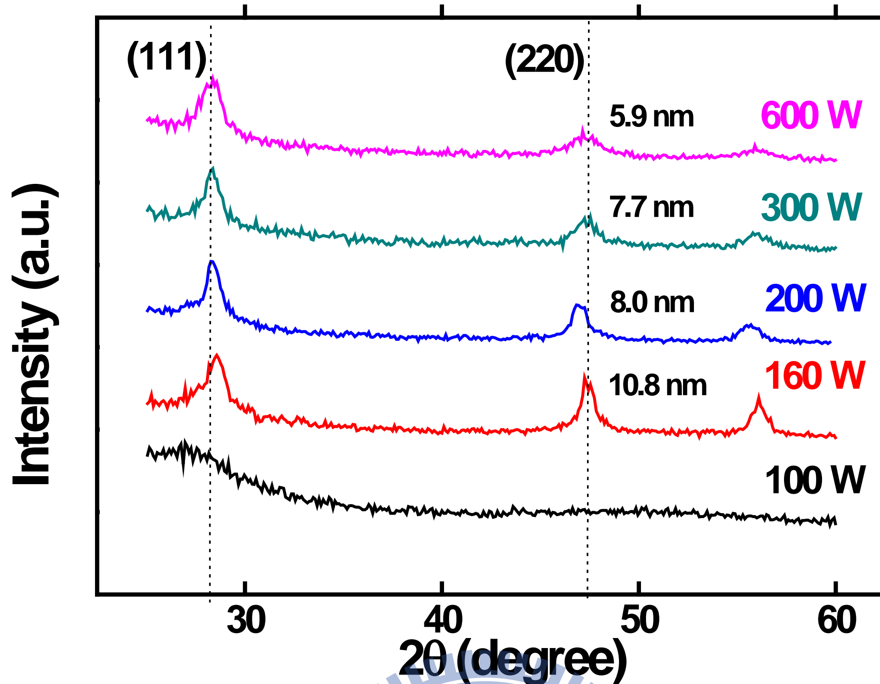

Fig 4.22 XRD spectra of μc-$Si_{1-x}Ge_x$ films deposited on bare glass at fixed germane concentration (R_{GeH_4}) with various power ranging from 100 W to 600 W.

4.3.2 Effect of Hydrogen Dilution on Conductivity

Here we can see from **Fig 4.23** that when hydrogen dilution increased the crystallinity increased and then reached a saturation region. This is because when hydrogen dilution ratio increased, the amount of atomic hydrogen at growing surface is also increased. So the hydrogen etching effect is more pronounced and leading to higher crystallinity. Once the mount of atomic hydrogen reaches a threshold value at the growing surface, the ability to crystallize the film is the same for all hydrogen dilution. So film deposited at hydrogen dilution ratio of 95.3 % is close to the transition region. But there are also some powders formed. Therefore the best condition would be hydrogen dilution at 96.3 %, and we also need further improvement.

Compare **Fig 4.23** and **Fig 4.24**, the highly crystallized film reflect that there is no significant change in conductivities. The photo response is about one order for all the film, but the dark conductivity is a little bit too high Hence further improvement will be decreasing the crystallinity by lowing pressure.

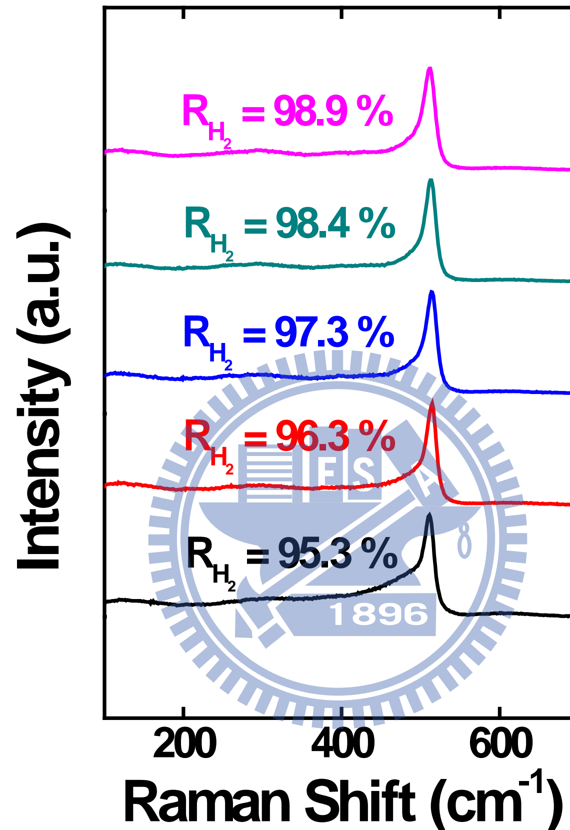

Fig 4.23 Raman scattering spectra of μc-$Si_{1-x}Ge_x$ films deposited on bare glass at different hydrogen dilution ratio (R_{H_2}) ranging from 95.3 % to 98.9 %. The other deposition parameters were kept unchanged.

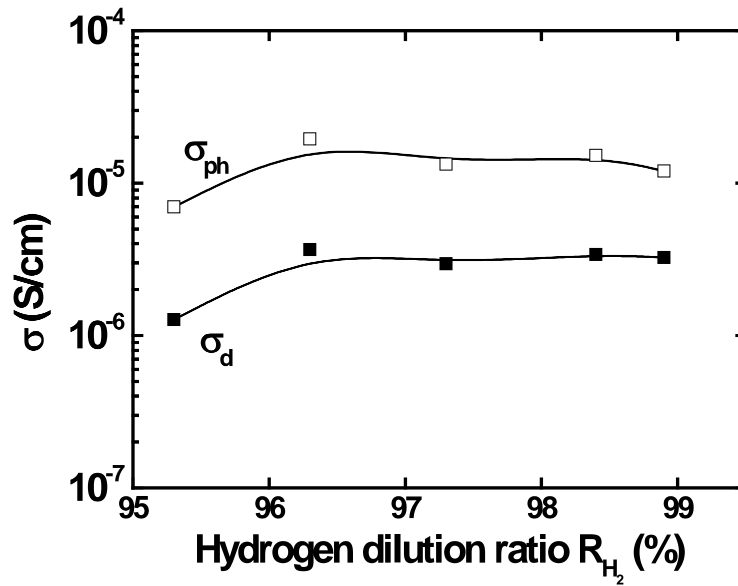

Fig 4.24 Dark conductivities (solid symbols) and photo conductivities (open symbols) as a function of hydrogen dilution ratio (R_{H_2}).

4.3.3 Effect of GeH_4 Concentration on Conductivity

Fig 4.25 represents that as germanium content increased, the Si-Si peak shifted toward small wavenumber because of the presence of nearby germanium atom. And the Si-Ge bond becomes more pronounced as GeH_4 concentration increases. Furthermore, Addition of germanium atom will deteriorate crystallization as we can see from the broadened peak of the Raman spectra. On one hand we hope to increase absorption coefficient by adding germanium atom, on the other hand the addition of geranium atom will induce defect formation and therefore deteriorate the crystallinity. So how to control certain amount of germanium atom in the film is a tradeoff.

We can observer from **Fig 4.26** that as germanium content increases, the photo response increases, too. And the photo response reaches two order of magnitude in GeH_4 concentration between 9.1 % to 16.7 %, which is suitable for a device quality μc-SiGe:H material. Moreover, we can see that when germanium content increases

the dark conductivity drops 5 orders in magnitude that means the film transform from crystalline to amorphous. This also agreed with the results from **Fig 4.25**.

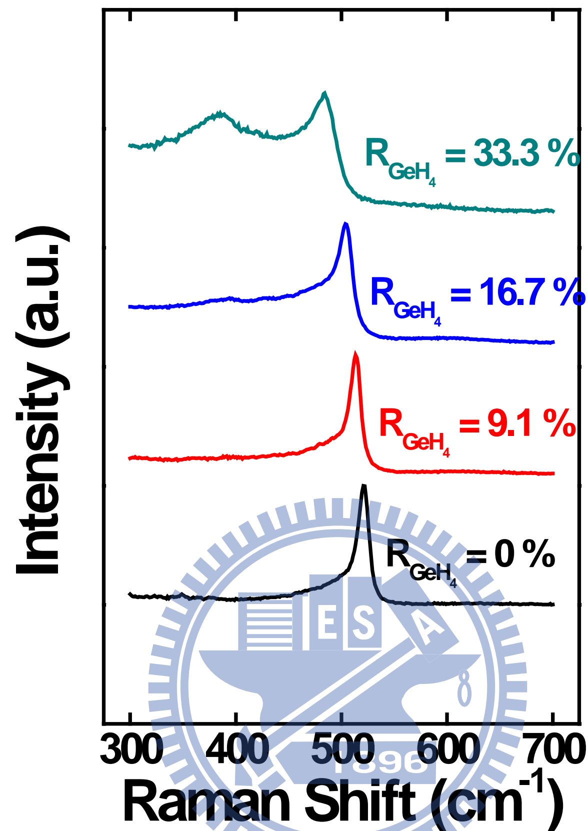

Fig 4.25 Raman scattering spectra of μc-$Si_{1-x}Ge_x$ films deposited on bare glass at different germane concentrations (R_{GeH_4}) ranging from 9.1 % to 33.3 %. The μc-Si:H film is also shown for comparison.

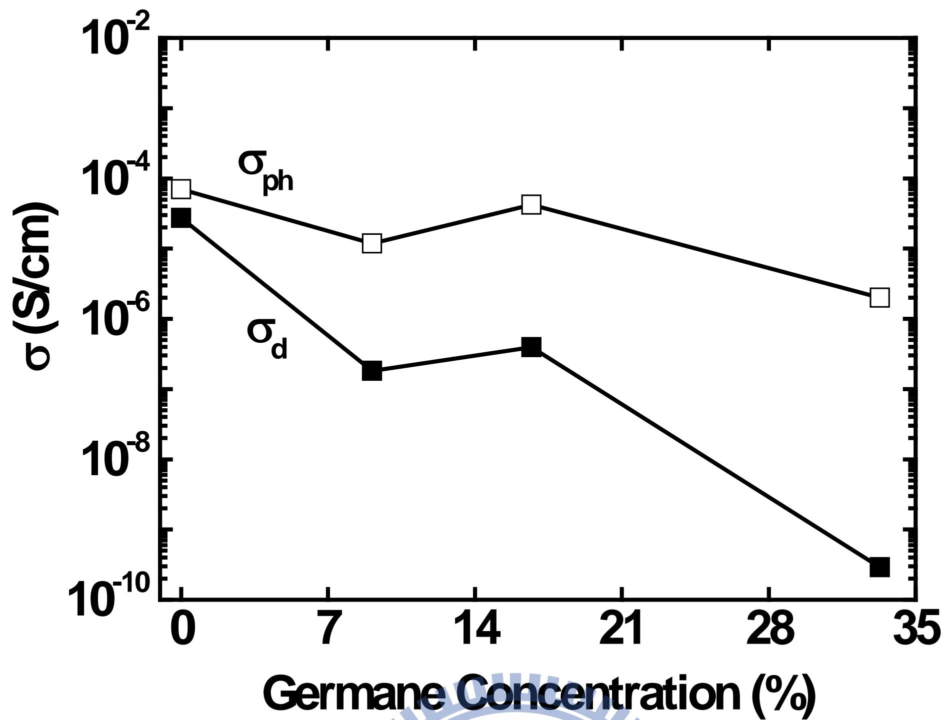

Fig 4.26 Dark conductivities (solid symbols) and photo conductivities (open symbols) as a function of germane concentration (R_{GeH_4}).

Fig 4.27 represents that as germanium concentration increased the Si-Ge peak at 400 cm^{-1} and Ge-Ge peak at 300 cm^{-1} also rose. And the Ge-Ge peak rises more than the Si-Ge peak that means Ge atom tends to aggregate with each other, which is unwanted for alloy formation. Therefore, we should minimize the Ge-Ge bonding and maximize the Si-Ge bonding to form a valid Si-Ge alloy.

Fig 4.28 shows that there are two factors competes each other. First, when the amount of GeH_4 concentration is low, the photo response becomes small as we increase the GeH_4 concentration. That is because we keep the total hydrogen dilution ratio unchanged as we increase GeH_4 concentration but the hydrogen dilution of Si is slightly increased. So the dark-conductivity will rise as GeH_4 concentration increase. Second, when GeH_4 concentration increase further, both the photo- and

dark-conductivity decrease and the photo response become larger, which is due to incorporating germanium atom will deteriorate the crystalline formation.

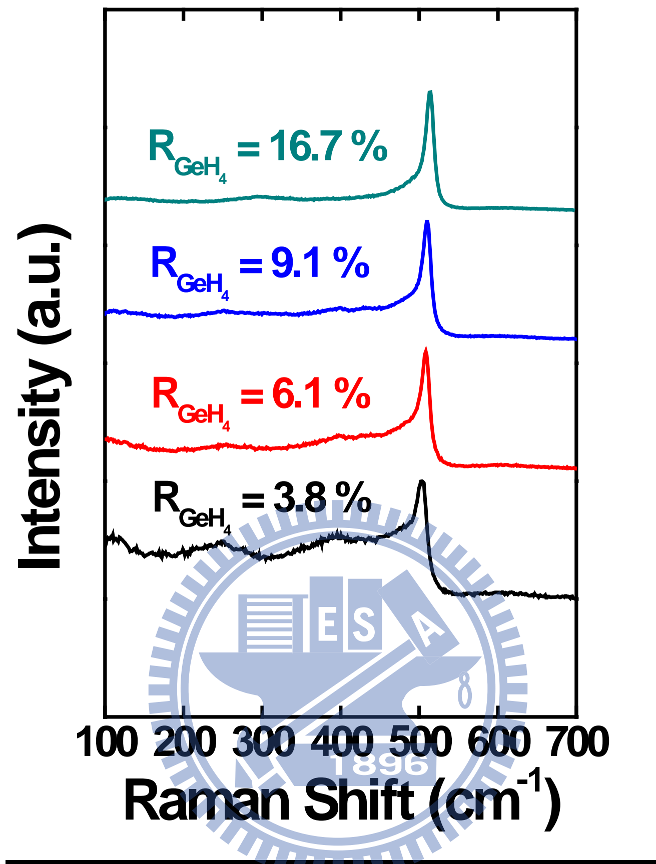

Fig 4.27 Raman scattering spectra of μc-$Si_{1-x}Ge_x$ films deposited on bare glass at different germane concentrations (R_{GeH_4}) ranging from 3.8 % to 16.7%.

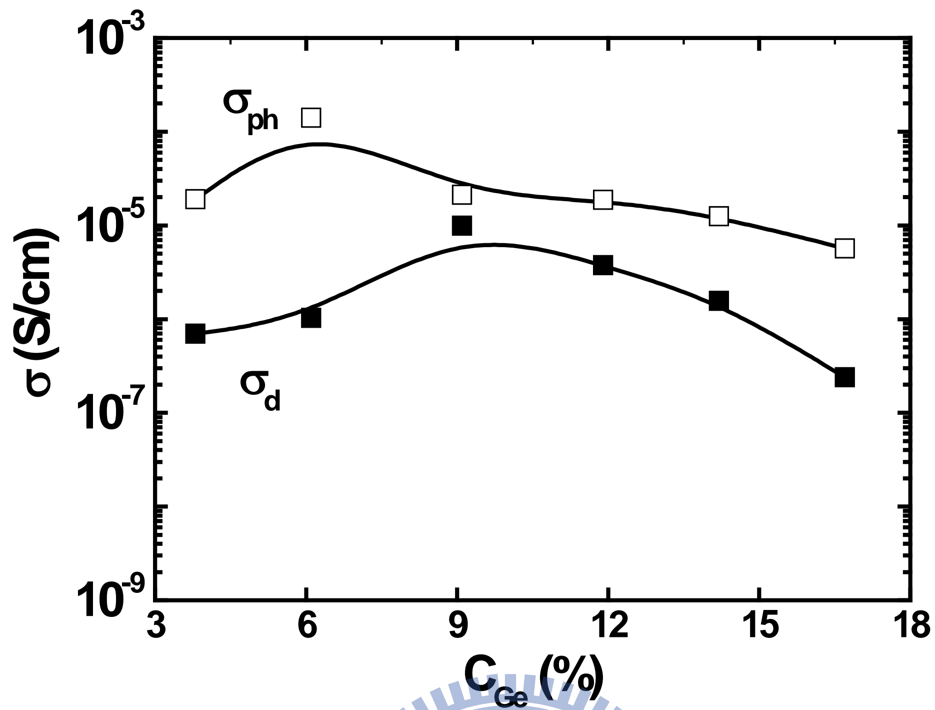

ES A 1896

Fig 4.28 Dark-conductivities (solid symbols) and photo-conductivities (open symbols) as a function of germane concentration (R_{GeH_4}).

Chapter 5 Conclusions

In this thesis, two major parts of experiments are performed, one is the investigation of a-SiGe:H thin-films properties and single junction solar cell optimization; another is the characterizations of μc-SiGe:H thin-films. In the first part, we examined the effect of hydrogen dilution on film quality and compare them with each other. Here we summarize some conclusions from the results and comparisons and shown them as follows: when depositing a-SiGe:H thin-films, the hydrogen dilution will improve the film quality and facilitate the germanium incorporation. This is due to the hydrogen etching effect and the more efficient dissociation of GeH_4 molecules in a hydrogen-rich environment respectively. The hydrogen etching model can also be verified from the observation of the decrease of deposition rate as the hydrogen dilution is increased. Meanwhile, the hydrogen etching cannot be too severe otherwise it may induce more defects formed during deposition. Therefore, we should deposit films within a proper hydrogen dilution region to get a better film quality.

In the aspect of a-SiGe:H single junction solar cells, only some important points will be mentioned here. First, the most suitable i-layer thickness will change with germanium content in the film, the more Ge incorporation in the film, the thinner i-layer thickness. Generally speaking, the i-layer thickness should be in the range of 150 nm to 300 nm. Second, although a-SiGe:H thin-films deposit at 30 W is higher in photo response than thin-films deposit at 20 W, but cell performance are lower when i-layer is deposited at 30W. One of the possible reasons is that high RF power will enhance the ion bombardment, which in turn causes some damage at the growing

surface and deteriorate film quality. Thus, we should avoid too much ion bombardment and operate in a relatively low power region despite that the film shows better characteristics.

In the second part, we discuss the relation of RF power, hydrogen dilution and germane concentration on microcrystalline silicon germanium (μc-SiGe:H) film properties. The amorphous to microcrystalline transition appears when rf power is about 200 W and accompanied with the drastically increased conductivities. The rise of dark conductivities indicates the formation of micro-crystallites and also represents increased defect density within the grain boundary, while photo response should be as high as possible. The general photo conductivities shall be about 1.5 to 2 orders. Moreover, the grain size increased when the film approaches to transition region.

By changing hydrogen dilution ratio, we can approach the transition between amorphous phase to microcrystalline phase, and control the crystallinity of μc-SiGe:H thin-films. The sharp c-Si peak and on-order photo response indicate the film is highly crystallized, and may induce too much defects.

The SiGe material quality is largely dominated by the germanium content in SiGe thin-films, alloying with germanium will enhance the absorption coefficient and narrow the bandgap but it will create more defects within the material as well. The μc-SiGe:H thin-films attained device quality is the film with photo response nearly 1.5 to 2 orders, which is in the range of germane concentration of 9.1 % to 16.7 %.

Chapter 6 Future Works

Although we had made some progress in the cell performances of a-SiGe:H single junction solar cells, but the cell is still far from perfection because there exist some problems that hinders the further application of these a-SiGe:H solar cells. The first one is the quantum efficiency of a-SiGe:H solar cells. As discussed in the content, the absorption of long-wavelength region is weak even when Ge content (C_{Ge}) is up to 30%, which limits the application of a-SiGe:H as a bottom cell material in a tandem cell structure. Due to the concept of spectrum splitting, the current share (the overlapping area of a-Si:H top cell and a-SiGe:H bottom cell) between top cell and bottom cell should be minimized, which means the separation of absorption peaks of two sub-cells is enough to absorb wider spectrum. Therefore, our first goal is to further enhance the absorption in the long-wavelength region, so that we can improve the cell efficiency of tandem solar cells. In order to enhance the absorption, the properties of a-SiGe:H thin-films should be carefully checked and further fine tune of deposition parameters is needed. Also, the germanium content should be elevated and meanwhile keep the film quality. Furthermore, the p-layer properties can be re-optimized and try to increase the conductivities of these doped layers.

After solving the problem of absorption range, then the a-SiGe:H cell can be applied to tandem structure solar cells. In the tandem region, there is still a huge area that we can investigate such as the tunneling recombination junction (TRJ) and the current matching issues…etc.

As for μc-SiGe:H thin films, the fundamental problem is the formation of

powders during the deposition process. The formation of these powders can be originated from two possibilities, one is the severe gas phase reaction due to the film is deposited in high hydrogen dilution region; another is the peeling from the pre-deposition film arise from the weak adhesion of μc-SiGe:H films on the pre-deposition film. The second possibility had already been tested and verified, for the changing of pre-deposition parameters will largely decrease the formation of powders. Thus, the pre-deposition parameters should be re-optimized for deposition in the microcrystalline region and meanwhile to avoid too much gas phase reaction so that the proper conditions for μc-SiGe:H thin-films can be located.

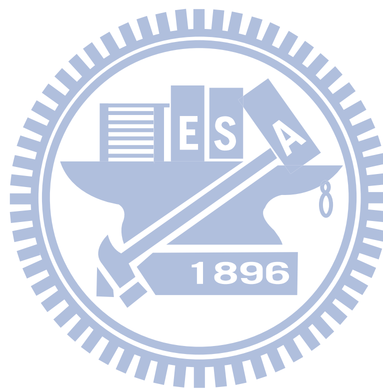

Chapter 7 References

[1] I. Repins, M. Contreras, B. Egaas, C. DeHart, J. Scharf, C. Perkins, B. To, and R. Noufi, "Short Communication: Accelerated Publication 19¡P 9%-efficient ZnO/CdS/CuInGaSe2 solar cell with 81¡P 2% fill factor," *Progress in Photovoltaics: Research and Applications,* vol. 16, pp. 235-239, 2008.

[2] H. Chen, J. Hou, S. Zhang, Y. Liang, G. Yang, Y. Yang, L. Yu, Y. Wu, and G. Li, "Polymer solar cells with enhanced open-circuit voltage and efficiency," *Nature Photonics,* vol. 3, pp. 649-653, 2009.

[3] K. Yamamoto, A. Nakajima, M. Yoshimi, T. Sawada, S. Fukuda, T. Suezaki, M. Ichikawa, Y. Koi, M. Goto, and T. Meguro, "A thin-film silicon solar cell and module," *Progress in Photovoltaics: Research and Applications,* vol. 13, pp. 489-494, 2005.

[4] T. Roschek, "Microcrystalline silicon solar cells prepared by 13.56 MHz PECVD," 2003.

[5] H. Sterling and R. Swann, "Chemical vapour deposition promoted by rf discharge," *Solid-State Electronics,* vol. 8, pp. 653-654, 1965.

[6] W. Spear and P. Le Comber, "Substitutional doping of amorphous silicon," *Solid State Communications,* vol. 88, pp. 1015-1018, 1993.

[7] D. Carlson and C. Wronski, "Amorphous silicon solar cells," *Amorphous Semiconductors,* pp. 287-329, 1979.

[8] D. Staebler and C. Wronski, "Reversible conductivity changes in discharge produced amorphous Si," *Applied Physics Letters,* vol. 31, p. 292, 1977.

1896

[9] M. Stutzmann, W. Jackson, and C. Tsai, "Light-induced metastable defects in hydrogenated amorphous silicon: A systematic study," *Physical Review B,* vol. 32, pp. 23-47, 1985.

[10] A. Matsuda, M. Takai, T. Nishimoto, and M. Kondo, "Control of plasma chemistry for preparing highly stabilized amorphous silicon at high growth rate," *Solar Energy Materials and Solar Cells,* vol. 78, pp. 3-26, 2003.

[11] R. Schropp and M. Zeman, *Amorphous and microcrystalline silicon solar cells: modeling, materials, and device technology*: Kluwer Academic Publishers, 1998.

[12] P. Voyles, J. Gerbi, M. Treacy, J. Gibson, and J. Abelson, "Absence of an abrupt phase change from polycrystalline to amorphous in silicon with deposition temperature," *Physical review letters,* vol. 86, pp. 5514-5517, 2001.

[13] D. Staebler and C. Wronski, "Reversible conductivity changes in discharge-produced amorphous Si," *Applied Physics Letters,* vol. 31, pp. 292-294, 1977.

[14] C. Tsai, G. Anderson, R. Thompson, and B. Wacker, "Control of silicon network structure in plasma deposition," *Journal of Non-Crystalline Solids,* vol. 114, pp. 151-153, 1989.

[15] S. Vep ek, Z. Iqbal, and F. Sarott, "A thermodynamic criterion of the crystalline-to-amorphous transition in silicon," *Philosophical Magazine Part B,* vol. 45, pp. 137-145, 1982.

[16] T. Akasaka and I. Shimizu, "In situ real time studies of the formation of polycrystalline silicon films on glass grown by a layer by layer technique," *Applied Physics Letters,* vol. 66, p. 3441, 1995.

[17] G. Ganguly, T. Ikeda, T. Nishimiya, K. Saitoh, M. Kondo, and A. Matsuda,

ES A 1896

"Hydrogenated microcrystalline silicon germanium: A bottom cell material for amorphous silicon based tandem solar cells," *Applied Physics Letters,* vol. 69, p. 4224, 1996.

[18] M. Isomura, K. Nakahata, M. Shima, S. Taira, K. Wakisaka, M. Tanaka, and S. Kiyama, "Microcrystalline silicon-germanium solar cells for multi-junction structures," *Solar energy materials and solar cells,* vol. 74, pp. 519-524, 2002.

[19] S. Miyazaki, H. Takahashi, H. Yamashita, M. Narasaki, and M. Hirose, "Growth and characterization of microcrystalline silicon-germanium films* 1," *Journal of Non-Crystalline Solids,* vol. 299, pp. 148-152, 2002.

[20] T. Matsui, K. Ogata, M. Isomura, and M. Kondo, "Microcrystalline silicon-germanium alloys for solar cell application: Growth and material properties," *Journal of Non-Crystalline Solids,* vol. 352, pp. 1255-1258, 2006.

[21] T. Matsui, H. Jia, and M. Kondo, "Thin film solar cells incorporating microcrystalline Si1-xGex as efficient infrared absorber: an application to double junction tandem solar cells," *Progress in Photovoltaics: Research and Applications,* vol. 18, pp. 48-53, 2010.

[22] T. Matsui, M. Kondo, K. Ogata, T. Ozawa, and M. Isomura, "Influence of alloy composition on carrier transport and solar cell properties of hydrogenated microcrystalline silicon-germanium thin films," *Applied Physics Letters,* vol. 89, p. 142115, 2006.

[23] R. Carius, J. Folsch, D. Lundszien, L. Houben, and F. Finger, "Microcrystalline silicon-germanium alloys for absorption layers in thin film solar cells," 1999, pp. 813-818.

[24] C. Raman and K. Krishnan, "A new type of secondary radiation," *Nature,* vol. 121, p. 501, 1928.

1896

[25] D. Long, *Raman spectroscopy*: McGraw-Hill New York, 1977.

[26] R. McCreery, *Raman spectroscopy for chemical analysis*: Wiley-Interscience, 2000.

[27] M. Islam and S. Kumar, "Influence of crystallite size distribution on the micro-Raman analysis of porous Si," *Applied Physics Letters,* vol. 78, p. 715, 2001.

[28] R. Kobliska and S. Solin, "Raman spectrum of wurtzite silicon," *Physical Review B,* vol. 8, pp. 3799-3802, 1973.

[29] M. Luysberg, P. Hapke, R. Carius, and F. Finger, "Structure and growth of hydrogenated microcrystalline silicon: investigation by transmission electron microscopy and Raman spectroscopy of films grown at different plasma excitation frequencies," *Philosophical Magazine A,* vol. 75, pp. 31-47, 1997.

[30] R. Street, *Hydrogenated amorphous silicon*: Cambridge Univ Pr, 1991.

[31] T. Searle, "Properties of amorphous silicon and its alloys," *Engineering Science and Education Journal,* vol. 9, pp. 4-4, 2000.

[32] A. Mahan, P. Raboisson, and R. Tsu, "Influence of microstructure on the photoconductivity of glow discharge deposited amorphous SiC: H and amorphous SiGe: H alloys," *Applied Physics Letters,* vol. 50, pp. 335-337, 1987.

[33] W. Lau, *Infrared characterization for microelectronics*: World Scientific Pub Co Inc, 1999.

[34] B. Cullity, "Elements of X-ray Diffraction," *Massachusetts, USA,* 1977.

[35] Y. Hishikawa, N. Nakamura, S. Tsuda, S. Nakano, Y. Kishi, and Y. Kuwano, "Interference-free determination of the optical absorption coefficient and the optical gap of amorphous silicon thin films," *Japanese journal of applied*

physics, vol. 30, pp. 1008-1014, 1991.

[36] M. Goerlitzer, P. Torres, N. Beck, N. Wyrsch, H. Keppner, J. Pohl, and A. Shah, "Structural properties and electronic transport in intrinsic microcrystalline silicon deposited by the VHF-GD technique," *Journal of Non-Crystalline Solids,* vol. 227, pp. 996-1000, 1998.